3'UTR Remodelling of Axonal Transcripts in Sympathetic Neurons

Catia Andreassi[1,5], Raphaëlle Luisier[3,5], Hamish Crerar[1], Sasja Franke[1], Nicholas M. Luscombe[2,3], Giovanni Cuda[4], Marco Gaspari[4] and Antonella Riccio[1]

[1] MRC Laboratory for Molecular Cell Biology and [2]UCL Genetics Institute, University College London, London, WC1E 6BT, UK, [3]Francis Crick Institute, London, NW1 1AT, UK and [4] Department of Experimental and Clinical Medicine, University Magna Graecia, Catanzaro, 88100, Italy

[5]These authors contributed equally to the study

[¶]To whom correspondence should be addressed Email: a.riccio@ucl.ac.uk

Asymmetric localization of mRNAs is a mechanism that constrains protein synthesis to subcellular compartments. In neurons, mRNA transcripts are transported to both dendrites and axons where they are rapidly translated in response to extracellular stimuli. To characterize the 3'UTR isoforms localized in axons and cell bodies of sympathetic neurons we performed 3'end-RNA sequencing. We discovered that isoforms transported to axons had significantly longer 3'UTRs compared to cell bodies. Moreover, more than 100 short 3'UTR isoforms were uniquely expressed in axons. Analysis of the long 3'UTR of *IMPA1* indicated that a multiprotein complex including Upf1, HuD and Ago2 mediated 3'UTR cleavage. This event enhanced *IMPA1* translation and was necessary for maintaining axon integrity. 3'UTR cleavage took place in axons and was not limited to *IMPA1* but extended to other transcripts with similar expression patterns. We conclude that the 3'UTR of neuronal transcripts undergo post-transcriptional remodelling and describe an alternative mechanism that regulates local protein synthesis

KEYWORDS

3'UTR remodelling; sympathetic neurons; RNA localization; axons; alternative polyadenylation; local protein synthesis

HIGHLIGHTS

- 3'end-Seq reveals distinct expression of alternative 3'UTR isoforms in axons and cell bodies of sympathetic neurons.
- Short 3'UTR isoforms uniquely detected in axons are generated *in situ* by cleavage of longer precursors.
- A protein complex containing Upf1, HuD, Pabpc4 and Ago2 mediates the cleavage of 3'UTRs.

INTRODUCTION

Neurons are cells with a complex morphology, which maintain their cellular structure through the compartmentalized expression of proteins essential for growth and plasticity. Asymmetric localization of RNA is an evolutionarily conserved mechanism that allows spatial restriction of protein synthesis to specific cellular compartments. Incorrect processing and delivery of mRNA causes developmental defects and severe human neurological disorders (Holt and Schuman, 2013; Wang et al., 2007). Eukaryotic mRNAs share common features that include exons and introns, 5' and 3' untranslated regions (UTRs), a modified base at the 5' end named "cap", and a stretch of adenosines at the 3' end named poly(A) tail, which confers stability to the transcript preventing premature degradation and enables its translation. The information necessary for RNA processing can be stored anywhere along the transcript, however most elements that regulate mRNA transport and translation are found within the 3' and 5'UTRs. 3'UTRs regulate multiple aspects of mRNA metabolism, including nuclear export, cytoplasmic localization, translational efficiency and mRNA stability, while the 5'UTR is primarily involved in controlling mRNA translation (Andreassi and Riccio, 2009; Hinnebusch et al., 2016).

During neuronal development, transcripts are transported to both dendrites and axons, where they are rapidly translated in response to external cues (Holt and Schuman, 2013; Martin and Ephrussi, 2009). A number of studies have shown that stimulus-induced axonal translation of mRNAs is necessary for axon growth, axon steering and regeneration (Baleriola et al., 2014; Ben-Yaakov et al., 2012; Colak et al., 2013; Leung et al., 2006; Shigeoka et al., 2016; Yao et al., 2006). In sympathetic and sensory neurons for example, hundreds of transcripts are targeted to axons in response to Nerve Growth factor (NGF), which is necessary for both neuronal survival and differentiation (Andreassi et al., 2010; Willis et al., 2005). A localization element was first identified within the 3'UTR of β-actin and was named "zipcode" because it was necessary for delivering *β-actin* mRNA to the

leading lamellae of fibroblasts and to dendrites (Eom et al., 2003; Kislauskis et al., 1994). Following this seminal discovery, many localization elements have been found within the 3'UTRs of transcripts transported to both dendrites and axons. In sympathetic neurons, a localization element within the 3'UTR is necessary and sufficient to target the *IMPA1* transcript to axons in response to NGF (Andreassi et al., 2010). Similarly, a 3'UTR variant of *importin-β1* is responsible for axonal targeting of the transcript and for activating the injury response in adult sensory neurons (Perry et al., 2012). In hippocampal neurons, isoforms of the *BDNF* transcript with either short or long 3'UTRs are localized to dendrites in response to extracellular cues (Allen et al., 2013; An et al., 2008; Will et al., 2013).

3'UTRs recruit RNA binding proteins (RBPs) through sequence-specific interactions, thereby generating multi-protein complexes with flexible functions (Singh et al., 2015). RBP complexes are assembled on the nascent mRNA, but along the way they change in composition to add proteins that mediate mRNA splicing, nuclear export and localization. Interestingly, RBPs may serve as molecular hubs that regulate axonal trafficking and local synthesis of functionally related mRNAs. The Splicing Factor Poly-Glutamine rich (SFPQ) protein for example, recognises a localization element present in a number of 3'UTRs that allows the coordinated transport of transcripts to sensory and motor neuron axons (Cosker et al., 2016) (Thomas-Jinu et al., 2017). Despite these recent findings however, the role of 3'UTRs in regulating mRNA metabolism remains largely unknown.

We performed 3'end sequencing of mRNA isolated from either cell bodies or axons of sympathetic neurons and found that thousands of 3'UTR isoforms are expressed in axons. Interestingly, over 100 shorter 3'UTR isoforms were either highly enriched or uniquely detected in axons, suggesting that they are not transported from the cell bodies and may have been generated *in situ*. Analysis of *IMPA1* transcripts, which are expressed in axons and encode a protein essential for maintaining axonal integrity (Andreassi et al., 2010), confirmed that an isoform bearing a short 3'UTR (*IMPA1-SS*) could not be targeted to

axons and was generated *in situ* by 3'UTR cleavage of the longer isoform *IMPA1-L*. *IMPA1-SS* is polyadenylated and efficiently translated, underscoring the critical role of 3'UTR remodelling in enhancing protein synthesis. Cleavage of *IMPA1-L* 3'UTR was mediated by a multi protein complex that includes the RNA helicase Upf1, the RNA binding protein HuD and Ago2, the binding partner of short interfering and other small RNAs. A handful of recent studies demonstrated distinct expression patterns of 3'UTRs and coding sequences for thousands of neuronal (Kocabas et al., 2015) and non neuronal (Mercer et al., 2011) genes. Because 3'UTRs do not originate from independent transcriptional events (Mercer et al., 2011), it has been suggested that a yet unknown mechanism mediating the remodelling of 3'UTRs may occur post-transcriptionally. Here, we provide evidence that cleavage of 3'UTRs takes place in sympathetic neuron axons and demonstrate the impact of 3'UTR remodelling on local protein synthesis and in maintaining axon integrity.

RESULTS

3'end-RNASeq of transcripts in axons and cell bodies of sympathetic neurons

To characterize the 3'UTRs of transcripts localized in cell bodies or axons of rat sympathetic neurons, we performed stranded 3'end-RNASeq using mRNA isolated from neurons grown in compartmentalized chambers (**Figure S1A**). In this model system, distal axons are separated from the cell bodies by a 1 mm wide Teflon divider, allowing the isolation of mRNA from distinct cellular compartments. Prior to sequencing, mRNA was subjected to two rounds of linear amplification (**Figure S1B**) that generated anti-sense RNA. Although the samples were not suitable for conventional poly(A) sequencing, the linear amplification led to the accumulation of reads at the 3' end of transcripts (**Figure S1C**), generating a read coverage profile similar to Poly(A)-Seq (Shepard et al., 2011). Because at least 65% of the reads accumulated in the last 500 nts of 3'UTRs irrespective of the transcript length, reads in these regions were used to measure 3'UTR isoform usage (**Figure 1A** and **Figure S1C**). The rat genome is poorly annotated compared with the mouse and human genomes, therefore RNA-Seq data were used to identify novel isoforms by re-annotating the 3' ends to the Ensembl Rn5 database (v78). A segmentation algorithm was used to recognise regions of continuous coverage, which are expected to coincide with genuine alternative 3'UTRs (**Figure 1B**). Using this method, we identified 26,468 new 3'UTR isoforms in addition to existing Ensembl annotations, and extended the 3'UTR length for 7,506 transcripts (**Figure 1C** and **Figure S1D**). The reliability of these annotations was assessed by checking them against a comprehensive polyadenylation atlas compiled from a variety of independent sources, which include a) known 3' end termini from RefSeq (Rn5 and Rn6) and Ensembl (Rn6), b) previously reported polyA sites from PolyA-DB2 (Lee et al., 2007) and APADB (Muller et al., 2014) , and c) PAS obtained from 3'-Seq data obtained from rat and human samples (Derti et al., 2012; Gruber et al., 2016). Up to nearly 70% of newly identified 3' ends in our dataset were found within 100

nts distance of annotations in these resources, demonstrating the suitability of our approach (**Figure 1D** and **Figure S1E-G**). Over 80% of previously annotated transcripts and around 67% of the extended 3'UTRs contained a PAS within 150 nts of the 3'end, with non-canonical PAS motifs being most frequently used. Longer isoforms showed a higher frequency of non-canonical PAS motifs such as AAGAAA and GATAAA (**Figure 1E** and **1F**). Greater enrichment of predicted PASs was observed with increasing 3'UTR length, suggesting that transcripts bearing longer 3'UTRs are more likely to generate multiple isoforms (**Figure 1G**). To further confirm that re-annotated transcripts were genuinely expressed isoforms, 3' rapid amplification of complementary DNA end (3'RACE) was performed for the *actin beta*, *stathmin 2* and *Cofilin1* transcripts. For all transcripts analysed the 3'RACE isoforms matched the 3' ends identified by the screen (**Figure 1H** and **1I**). Based on these findings, we concluded that 3'end-RNASeq combined with *in silico* extension of 3'UTRs reliably allows the comprehensive identification of expressed 3'UTR isoforms.

Unique distribution of 3'UTR isoforms in axons and cell bodies

Distinct 3'UTRs are generated by alternative polyadenylation of the nascent mRNA, and the choice of poly(A) site is governed by tissue- and developmental stage-restricted factors (Lianoglou et al., 2013). To investigate whether specific 3'UTR isoforms were localized in axons or cell bodies, transcripts were divided into two categories, those present solely in cell bodies, or those present also in axons. Using this method 9,378 3'UTR isoforms associated with 6,410 transcripts, were located in axons (**Figure 2A** and **S2A** and **B**). Gene Ontology (GO) analysis of genes transcribing axonal mRNAs showed enrichment of terms related to neurotrophin signalling, protein trafficking and neuronal projections, whereas genes related to nuclear functions were overrepresented in the cell bodies (**Figure 2A**). Moreover, transcripts localised in axons contained remarkably longer 3'UTRs, when compared to transcripts restricted to cell bodies (**Figure 2B**). A larger

percentage of axonal transcripts presented multiple 3'UTR isoforms compared to cell bodies, with many transcripts showing three or more alternative 3'UTR isoforms (**Figure 2C**). Thus, axonal transcripts bear longer 3'UTRs and undergo a more complex regulation through alternative polyadenylation than cell body transcripts. Moreover, the inclusion of alternatively spliced last exons (ALE) has been recently shown to be over-represented in transcripts localized in neurite-like protrusions and identified by conventional RNA-Seq (Taliaferro et al., 2016).

Among transcripts with multiple isoforms, we compared the relative usage of promoter-proximal and promoter-distal poly(A) sites (Tian and Manley, 2013) between cell bodies and axons. Transcripts containing two or more 3'UTRs isoforms were considered for further analysis (4,191 tandem pairs of 3'UTR isoforms, **Figure 2D** and **Figure S2C**) and the difference in log2 proximal-to-distal expression ratios of 3'UTR isoforms between cell bodies and axons was calculated. A difference below -1 (FDR<0.01, Fisher count test) indicated a distal shift of poly(A) usage in axons, compared with cell body. We found 737 isoforms (17.7% of tandem 3'UTR isoforms) that displayed increased usage of distal 3'UTR isoforms in axons (**Figure 2D**, dark blue dots). Conversely, differences above 1 (FDR<0.01, Fisher count test) indicated a proximal shift of poly(A) usage in axons. Using these criteria, 689 shorter 3'UTR isoforms (16.5% of tandem isoforms) were found to be preferentially expressed in axons (**Figure 2D**, light blue dots). GO functional analysis revealed that terms associated with axon growth and energy and protein metabolisms were statistically overrepresented among axonal transcripts with shorter 3'UTRs, whereas terms associated with more general biological pathways, such as intracellular signalling, were enriched among axonal transcripts with longer 3'UTRs (**Figure 2E**).

Interestingly, by applying a thresholding method (see **Figure 2D** legend and Methods for details) a subset of transcripts displayed extreme differences in isoform usage: 63 transcripts with longer 3'UTR isoforms and 128 with shorter 3'UTR isoforms were either

uniquely detected or very highly expressed in axons (**Figure 2D**, inset). Lack of detection of some short isoforms in cell bodies may be due to the fact that they are generated co-transcriptionally by alternative polyadenylation and rapidly transported to axons. An alternative explanation however is that at least in some cases, long 3'UTRs are subjected to local remodelling in axons, which results in their cleavage and shortening. Examples of transcripts with strikingly distinct poly(A) usage in cell bodies or axons are shown in **Figure 2F** and **2G**, and in **Figure S2D** and **S2E**.

A short 3'UTR isoform of *IMPA1* is present only in axons

The finding that a number of shorter 3'UTR isoforms were detected solely in axons prompted us to investigate whether they may be the result of local remodelling. We previously discovered that *IMPA1* transcript is expressed in sympathetic neuron axons and that local translation is necessary for maintaining axon integrity (Andreassi et al., 2010). 3'end-RNASeq of *IMPA1* transcripts identified the previously known 3'UTR isoforms *IMPA1-S* (1128 nts), *IMPA1-L* (bearing an additional 120 nts sequence, 1248 nts) and a new isoform with a much shorter 3'UTR (*IMPA1-SS,* 582 nts) that was enriched in axons (**Figure 3A**). 3' RACE using mRNA isolated from cell bodies or distal axons of sympathetic neurons grown in compartmentalized chambers confirmed that *IMPA1-SS* was found only in axons (**Figure 3B**). The apparent discrepancy between RACE and the more sensitive 3'end-RNA Seq is possibly due to the fact that the cell bodies compartment also includes proximal axons, which may explain the detection of *IMPA1-SS*, albeit at much lower levels than in distal axons by 3'end RNA-seq. It should also be noted that the extended annotation did not allow a clear distinction between isoforms generated by the usage of PAS located at a distance shorter than 500 nts, making it impossible to distinguish *IMPA1-S* from *IMPA1-L*. Northern blot analysis of mRNA isolated from sympathetic neurons and PC12 cells confirmed that at least four isoforms of *IMPA1* are

present in both cell types, including *IMPA1-L*, *IMPA1-S*, *IMPA1-SS* and a shorter isoform (*IMPA1-N*) detected also by the 3'end-RNASeq (**Figure 3C**).

To test whether *IMPA1-SS* 3'UTR was transported to axons, we generated vectors containing a modified green fluorescent protein (myrdEGFP) and a sequence encoding the super-short *IMPA1* 3'UTR (*MyrdEGFP-IMPA1-SS*). MyrdEGFP is a myristoylated, destabilized form of GFP that is rapidly inserted in the plasma membrane upon translation, preventing the intracellular diffusion of the protein (Aakalu et al., 2001). Because of the short half-life (ca. 2 hours), myrdEGFP provides a reliable readout of mRNA transport and local translation. As a control, we used *myrdEGFP-IMPA1-L*, which is efficiently targeted to axons (Andreassi et al., 2010). Both m*yrdEGFP-IMPA1-SS* and m*yrdEGFP-IMPA1-L* were expressed at similar levels when transfected in PC12 cells (**Figure S3A** and **B**). Sympathetic neurons were electroporated with the indicated vectors and GFP protein was visualized by performing GFP immunostaining (**Figure 3D**). As previously shown when axons of sympathetic neurons were electroporated with *myrdGFP-IMPA1-L* the GFP signal was clearly detected up to 1600μm away from the cell bodies. In contrast, m*yrdGFP-IMPA1-SS* was restricted to cell bodies and proximal axons (**Figure 3D**), indicating that *IMPA1-SS* 3'UTR is incapable of targeting the transcript to distal axons and growth cones as it lacks the 120 nts localization sequence present in *IMPA1-L* (Andreassi et al., 2010).

***IMPA1* 3'UTR is remodelled and polyadenylated in axons**

Because *IMPA1-SS* cannot be transported to distal axons, we reasoned that it may derive from the cleavage of *IMPA1-L* 3'UTR. To test this hypothesis, we generated DNA vectors containing the coding region of the *firefly* gene and the 3'UTR of either *IMPA1-L*, *IMPA1-SS* or *IMPA1-L* mutated at the two proximal poly(A) sites (*firefly-IMPA1-L Δ poly(A)*). When PC12 cells were transfected with *firefly-IMPA1-SS* a band of the

expected size (2.3 Kb) was observed. However, when *firefly-IMPA1-L* was transduced into PC12 cells, two transcripts were detected, one of the expected size of *firefly-IMPA1-L* (2.9 Kb) and a second that co-migrated with *firefly-IMPA1-SS* (**Figure 4A**). The ratio between *IMPA1-SS* and *IMPA1-L* isoforms decreased remarkably when cells were transfected with *firefly-IMPA1-L∆ poly(A)*, indicating that mutation of *IMPA1-SS* poly(A) site inhibited the shortening of *IMPA1-L*. To rule out the possibility that the shortening of *firefly-IMPA1-L* observed in PC12 cells was due to nuclear alternative PAS choice, sympathetic ganglia explants were cultured *in vitro* for 10 days, then cell bodies were surgically removed and axons were exposed to cordycepin (2.5μM for 2.5 hours) (**Figure 4B**). Cordycepin is an analogue of adenosine that when incorporated in the poly(A) tail, induces synthesis termination due to the absence of a 3' hydroxyl moiety (Chen et al., 2008). Axons were exposed to cordycepin or left untreated, and *IMPA1-L* mRNA was measured by reverse transcription followed by quantitative PCR (RT-qPCR). Blocking of polyadenylation in severed axons resulted in a remarkable accumulation of *IMPA1-L,* probably due to decreased remodelling of *IMPA1-L* (**Figure 4C**).

Most 3'UTRs are polyadenylated co-transcriptionally in a two-step process that couples pre-mRNA cleavage with the synthesis of a poly(A) tail formed of 200 to 300 adenosine residues (Proudfoot, 2011). The length of the poly(A) tail correlates with stability and translational efficiency and is dynamically modulated by adenylation and deadenylation complexes present both in the nucleus and the cytoplasm (Jalkanen et al., 2014). To assess whether *IMPA1-SS* was efficiently polyadenylated, mRNA was isolated from PC12 cells and subject to Tag addition and poly(A) test (TA-PAT) (di Penta et al., 2009). A tagged oligo(d)T primer was used in combination with a forward primer that specifically annealead to the most 3' end region of *IMPA1* shared by all isoforms. Amplification of *IMPA1* poly(A) tail resulted in two distinct bands, one with a size compatible with *IMPA1-*

L 3'UTR (813 nts) and a second of the expected size of *IMPA1-SS* 3'UTR (147 nts) + polyA tail (**Figure 4D**). The *IMPA1-SS* band was remarkably broader than that of *IMPA1-L* because oligo(d)T primers annealed to multiple regions of the poly(A) sequence, indicating a longer poly(A) tail.

Endonucleolytic cleavage of *IMPA1* 3'UTR in axons

To explore the hypothesis that *IMPA1-L* remodelling in axons generates cleaved 3'UTR fragments, we performed 5'P-dependent RNA oligo-Mediated Ligation RT-PCR (RML RT-PCR). In this assay, the 5' phosphorylated ends of RNA fragments are ligated to a synthetic RNA tag and subject to random hexamer reverse transcription. Cleaved fragments are PCR amplified using primers matching the RNA tag and a region of IMPA1-L 3'UTR, cloned and sequenced (**Figure 5A**). 5'P-dependent RNA oligo-Mediated Ligation of mRNA isolated from severed axons (**Figure 5B**) revealed that most clones (18/20, or 90%) contained an insert amplified from the cleaved 3'UTR of *IMPA1-L*. Remarkably, fragments were very homogenous in size and mapped to 17nts located downstream of the predicted cleavage site (expected size of the insert 294bps, average length 267.4±45.2, 5'end located]-44,+172[nts from the putative cleavage site) (**Figure 5B**, upper and lower panel). A similar result was observed when RNA was purified from total sympathetic neurons cultures (**Figure 5C**, upper panel). In addition to *IMPA1*, cleaved fragments for *Sms* and *Maoa*, which are two transcripts also showing a marked shift toward proximal poly(A) site usage in axons, were easily detected (*Maoa* 3'UTR (14 out of 14 clones, expected size of the insert 138bps, average length 88.7±33.8, 5'end located]-9,+89[bps from the putative cleavage site; *Sms* 3'UTR (17 out of 18 of the clones, expected size of the insert 357 bps, measured average length 258.3±44.0 bps, 5'end located]+64,+172[nts from putative cleavage site) (**Figure 5C**, middle and lower panels, and **Figure S2E**). As expected, 3'UTR cleavage was not detected in transcripts that did not show alternative poly(A) site usage, such as *Cops3*, *Fdxr* and *Maf1* (**Figure 5D** and

Figure S2F). It should be noted that the substantial lack of fragments whose 5' end was located upstream of the cleavage site indicates that these fragments are not an intermediate product of 5'-3' exonucleotic degradation. Thus, we conclude that *IMPA1-L* is capable of generating the shorter and efficiently polyadenylated isoform *IMPA1-SS* in a remodelling process of the 3'UTR that takes place in axons independently of nuclear alternative polyadenylation.

Inhibition of *IMPA1-L* 3'UTR remodelling decreases *IMPA1* translation

To investigate whether axonal remodelling of *IMPA-1* 3'UTR may be necessary to remove elements that maintain the transcript translationally repressed, we first performed luciferase reporter assays. PC12 cells were co-transfected with either *firefly-IMPA1-L*, *firefly-IMPA1-SS* or *firefly-IMPA1-LΔ poly(A)* and a *Renilla luciferase* vector, as a control for transfection efficiency. Quantification of luciferase activity indicated that *firefly-IMPA1-SS* was translated as efficiently as *firefly-IMPA1-L*. In contrast, mutation of the two proximal poly(A) sites of *IMPA1-L*, which impaired remodelling (**Figure 4A**) resulted in a 40% decrease of translation and this was not due to changes of mRNA levels (**Figure 6A** and **B**).

A more accurate measurement of translation is obtained by performing polysome fractionation, a technique that uses sucrose density gradients to separate mRNAs according to their association with either mono- or poly-ribosomes (Johannes and Sarnow, 1998). The absorbance profile of a representative experiment is shown in **Figure 6C**. PC12 cells expressing either *firefly-IMPA1-L*, *firefly-IMPA1-SS* or *firefly-IMPA1-LΔ poly(A)* were loaded on a 10-50% sucrose density gradient and mRNA was isolated from each fraction and analysed by northern blot. As a control, the housekeeping gene *GAPDH* was measured in the same fractions. Quantitative analysis of northern blots confirmed that both *firefly-IMPA1-L* and *firefly-IMPA1-SS* preferentially co-sediment with the polysome-

enriched fractions (**Figure 6D**). However, mutation of the proximal poly(A) sites induced a substantial shift of *firefly-IMPA1-L Δ poly(A)* toward the lighter, monosome-rich fractions. Thus, *IMPA1-SS* is translated as efficiently as *IMPA-1L* whereas the inhibition of *IMPA-1L* shortening to *IMPA1-SS* by mutating the proximal poly(A) sites decreases translation.

Local synthesis of *IMPA1* is necessary to maintain axon integrity in rat sympathetic neurons (Andreassi et al., 2010). To investigate whether *IMPA1-SS* was sufficient to rescue axon degeneration induced by *IMPA1* silencing, we generated vectors containing HA-tagged mouse *IMPA1* (*ms* HA-IMPA1) with either the long or the super-short 3'UTR of rat *IMPA1*. As expected, endogenous *IMPA1* levels were decreased when cells were transfected with siRNA that targeted the coding region of rat *IMPA1* (*IMPA1 tot* siRNA) or *IMPA1-L* isoform only *(IMPA1-L* siRNA) (**Figure S4A**). Transfection of *ms* HA-IMPA1-*rat* L rescued axon degeneration induced by *IMPA1 total* silencing (**Figure 6E**,**F** and **S4B**). Conversely, *ms* HA-IMPA1-*rat* SS, which cannot be transported to axons was incapable of rescuing axon degeneration induced by the silencing of either total *IMPA1* or *IMPA1-L*. When the 120 nts sequence required to target *IMPA1-L* to axons was cloned to the 3' of *IMPA1-SS* (*ms* HA-IMPA1-*rat* SS+120) and transduced in sympathetic neurons, we observed a complete rescue of axon degeneration induced by silencing of total *IMPA1* (**Figure 6E**,**F** and **S4B**). These findings confirm that *IMPA1-SS* 3'UTR lacks the localization elements necessary for axonal transport. They also show that when forcibly targeted to axons, *IMPA1-SS* is as efficient as *IMPA1-L* in maintaining axon integrity.

A Upf1 complex mediates *IMPA1-L* 3'UTR remodelling in axons

We next sought to identify the RNA binding proteins that may mediate *IMPA1* 3'UTR remodelling. Mass spectrometry analysis of RBPs associated with transcripts expressed in sympathetic neurons revealed that over two hundreds proteins interacted specifically with mRNA, with only a few recruited in a NGF-dependent manner (Aniko Ludanyi, M.G and A.R, unpublished observations). The DNA/RNA helicase Upf1 was one of the RBPs

that interacted with sympathetic neuron transcripts in response to NGF, a condition that is known to stimulate translation. Upf1 is part of the complex that mediates nonsense-mediated decay (NMD) of mRNA, a protein synthesis-dependent RNA surveillance pathway that prevents the translation of potentially deleterious truncated proteins by inducing rapid degradation of transcripts harbouring a premature termination codon (Kurosaki and Maquat, 2013). Binding of Upf1 is enriched on longer 3'UTRs and contributes to maintain mRNAs in a translationally silent state (Hurt et al., 2013). Western blotting of proteins extracts obtained from cell bodies or axons showed that Upf1 is detected in both compartments (**Figure 7A**). Because RBPs seldom function in isolation and are found within large multi-protein complexes, we performed mass spectrometry analysis of proteins that co-immunoprecipitated with Upf1 (**Figure S5A**). 325 unique peptides that mapped on 72 proteins were identified (**Figure 7B** and **Tables S1**, **S2** and **S3**), including known interactors of Upf1 (Polyadenylate-binding protein 1, ELAV-like protein 2, interleukin enhancer-binding factor 2, https://thebiogrid.org/111908/summary/homo-sapiens/upf1.html). Interestingly the neuron-specific ELAV protein ELAV-like protein 4 (or HuD) was one of the most abundant proteins that co-immunoprecipitated with Upf1. As for most RBPs, HuD regulates many aspects of RNA metabolism, including alternative splicing, alternative polyadenylation, mRNA stability and translation (Perrone-Bizzozero and Bird, 2013). The interaction of Upf1 with HuD and other RBPs identified by mass spectrometry analysis (protein argonaute-2 and Polyadenylate-binding protein 4) was confirmed in PC12 cells naïve and differentiated with NGF (**Figure 7C**). Similar results were observed when co-immunoprecipitation experiments were performed on sympathetic neurons (**Figure 7D**).

To study Upf1 and HuD binding to *IMPA1-L*, 3'UTR RNA immunoprecipitation (RIP) assay was performed in sympathetic neurons (**Figure 7E**). As a control, the binding of Upf1 to *Arf1* transcript, a well-known target of NMD, was also tested (**Figure S5B**). We

observed a robust interaction of Upf1 and HuD with *IMPA1-L* 3'UTR (**Figure 7E**). Importantly, inhibition of HuD/B, Ago2 and Pabpc4 expression decreased the cleavage of *IMPA1-L* 3'UTR. PC12 cells were transfected with siRNA targeting each mRNA and mRNA was isolated and subject to 5'P-dependent RNA oligo-Ligation Mediated RT-qPCR (**Figure 7F**). For each condition, a significant decrease of *IMPA1-L* 3'UTR cleavage, that was consistent with the efficiency of silencing, was observed (**Figure S5C**). Thus, we conclude that a RBP complex that includes Upf1 is responsible for the remodelling of *IMPA1* 3'UTR and possibly other transcripts.

DISCUSSION

The untranslated regions of mRNAs play a critical role in the regulation of transcript localization and translation in virtually all mammalian tissues. Global mapping of 3' ends regions indicated that around 75% of mammalian genes contain more than one poly(A) site (PAS), giving rise to multiple 3'UTRs (Proudfoot, 2011; Tian and Manley, 2013). Noticeably, PAS usage and 3'UTR length vary remarkably between mammalian tissues. Transcripts in the nervous system are characterized by significantly longer 3'UTRs, when compared to blood and testis, for example (Miura et al., 2013). Switch in the usage of PAS has been observed in a variety of biological processes. Proximal PASs are preferentially used in proliferating cells, in response to inflammation or in cancerous cells, where they generate transcripts with shorter 3'UTRs (Miura et al., 2013; Pai et al., 2016; Sandberg et al., 2008). Conversely, tissue differentiation is often associated with a switch from proximal to distal PAS and 3'UTR lengthening. In neurons, 3'UTR lengthening of a magnitude greater than in any other tissue takes place during development, with many transcripts bearing unusually long 3'UTRs (Miura et al., 2013) and alternative last exons (ALEs) (Taliaferro et al., 2016).

The 3'UTRs of axonal transcripts are longer and generate multiple isoforms

Our 3'end-RNASeq analysis on mRNA isolated from either cell bodies or axons of sympathetic neurons revealed a preferential usage of distal PAS and 3'UTR lengthening in transcripts localized in axons, when compared to cell bodies (**Figure 2B**). This may be due to the fact that elements within longer 3'UTRs are required for mRNA transport over long distances. A handful of transcripts have been shown to target axons and dendrites through elements contained within the 3'UTR. In sympathetic neurons for example, a 120 nts sequence at the 3'end of *IMPA1-L* 3'UTR is required for axonal localization in response to NGF (Andreassi et al., 2010). Similarly, the localization of *importin* β in sensory neurons depends on the presence of targeting elements within the longer 3'UTR (Perry et al., 2012).

We also observed that the number of PAS motifs increased with 3'UTR length (**Figure 1G**), and that a higher number of 3'UTR isoforms are expressed in axons (**Figure 2C**). Thus, in the nervous system, PAS choice plays an important role in determining the localization of transcripts. Moreover, the generation of multiple isoforms for the axonal transcriptome axons may contribute to finely tune protein synthesis in response to ever-changing environmental conditions.

Cleavage and remodeling of 3'UTRs in axons

Once transcripts have reached their peripheral destination they undergo local translation in response to physiological stimuli, including synaptic activation, neurotrophic factors and axon guidance cues (Holt and Schuman, 2013). In hippocampal neurons, a switch to proximal PAS usage and shortening of 3'UTRs was observed in genes that become transcriptionally activated in response to depolarization, perhaps indicating that a shorter 3'UTR enhances translation under these conditions (Flavell et al., 2008). Accordingly, we found 689 isoforms with shorter 3'UTR that were highly enriched in sympathetic neuron axons, when compared to cell bodies (**Figure 2D** and **2E**). Although in most instances these isoforms were detected also in cell bodies (albeit at much lower levels), at least 128 axonal transcripts with a shorter 3'UTR were virtually absent in cell bodies. An interpretation of these findings is that isoforms with a longer 3'UTR are generated by distal PAS usage in the nucleus and transported to axons where they undergo a remodeling process that gives rise to shorter 3'UTR isoforms. We cannot exclude however, that despite extensive sequencing (in excess of 80 million reads in each axon and cell body sample), isoforms uniquely detected in axons may be generated co-transcriptionally by proximal PAS usage and quickly transported to peripheral compartments.

PAS choice is thought to occur exclusively in the nucleus, where transcriptional elongation is coupled with 5' end capping, splicing of pre-mRNA, cleavage and polyadenylation of the 3' end (Tian and Manley, 2013). However, our findings indicate that at least for some transcripts, a remodeling of the 3'UTR takes place at the site of protein synthesis. Analysis of the *IMPA1* transcript revealed that an isoform bearing a shorter 3'UTR, *IMPA1-SS* (**Figure 3A-C**) was localized in distal axons despite lacking the localization element necessary for axonal targeting (**Figure 3D**). *IMPA-1-SS* is polyadenylated (**Figure 4C**) and efficiently translated (**Figure 6A-D**). When *IMPA1-SS*, which is normally restricted to cell bodies, was forcibly transported and expressed in axons, it rescued the axonal degeneration induced by IMPA1 silencing (**Figure 6E** and **F**). Importantly, we found that the 3'UTR of *IMPA1-L* undergoes cleavage in axons, generating *IMPA1-SS* and a 3'UTR fragment that was detected by 5' end RNA ligation (**Figure 5B**). These findings support a model (**Figure 7G**) by which *IMPA1-L* is transported to axons where the 3'UTR is remodeled into *IMPA1-SS* and translated in response to local extracellular cues. Cleavage of the 3'UTR was also shown for *Sms* and *Maoa* (**Figure 5C**), two transcripts that display preferential usage of proximal PAS site in axons (**Figure S2E**). Thus, remodeling of long 3'UTRs is a mechanism shared by many axonal transcripts that allows local protein synthesis.

An Upf1 complex mediates 3'UTR cleavage

How is 3'UTR remodeling regulated? We found that in sympathetic neurons, Upf1 binds to RNA in a NGF-dependent manner (Aniko Ludanyi, MG and AR unpublished observations), and that one of the targets was *Impa1-L* 3'UTR (**Figure 7E**). Upf1 is a helicase involved in NMD, a highly conserved mRNA surveillance pathway that targets transcripts harboring premature termination code for degradation (Nicholson et al., 2010). Though *IMPA1-L* is not a putative target of NMD (Hurt et al., 2013), Upf1 is recruited to long 3'UTRs (>1500 nts) of transcripts that lack the features normally associated with

sensitivity to NMD (Hogg and Goff, 2010; Hurt et al., 2013). Mass spectrometry analysis of proteins that co-immunoprecipitated with Upf1 revealed that HuD, Pabpc4 and Ago2 are part of a complex that mediate the cleavage of *IMPA1-L* 3'UTR (**Figure 7C-F**). A recent study has shown that maturation of miRNA precursors takes place in dendrites in response to depolarization (Sambandan et al., 2017). The finding that Ago2 and Pabpc4 are part of the 3'UTR remodeling complex suggests a potential cross-talk between local 3'UTR processing and miRNA machinery. Further investigation will be needed to elucidate the molecular mechanisms underlying Upf1-mediated remodeling of 3'UTRs and the potential signaling events that link environmental stimuli with 3'UTR cleavage.

A secret life for 3'UTRs?

The cleavage of 3'UTRs is not limited to *IMPA1* and was demonstrated for at least two other axonal transcripts, indicating that it may represent a general mechanism by which localized mRNA transcripts are translated in neurons. Remarkably, our cleavage assay demonstrated that in addition to shorter 3'UTR isoforms, intact fragments are generated as a byproduct of 3'UTR remodeling (**Figure 5B** and **C**). Widespread endonucleolytic post-transcriptional processing independent of miRNA targeting has been reported in mammalian cells (Karginov et al., 2010). Moreover, two recent studies have shown that 3'UTRs are expressed independently of their coding sequence. Mercer and colleagues demonstrated that in mouse, 3'UTR-derived RNAs (uaRNAs) are widely expressed in a tissue- and cell-specific manner (Mercer et al., 2011). It should be noted that genome-wide analysis of RNA Polymerase II binding revealed a lack of occupancy at these sites, indicating that they were not generated by transcriptional events originated from promoters located within the 3'UTRs (Mercer et al., 2011). Even more excitingly, differential expression of 3'UTRs and coding regions were observed for many genes expressed in the developing mouse brain (Kocabas et al., 2015). Here, we provide evidence for the mechanism that mediates the cleavage of 3'UTRs in sympathetic neurons, generating

remodeled 3'UTR isoforms and a new class of non-coding RNA fragments with yet unknown functions.

EXPERIMENTAL PROCEDURES

Reagents

Cell culture reagents, molecular biology reagents and kits were purchased from Thermo Fisher Scientific and all other chemicals from Sigma, unless stated otherwise.

Compartmentalized cultures of sympathetic neurons and SCG explants

All animal studies were approved by the Institutional Animal Care and Use Committees at University College London. Superior cervical ganglia were dissected from post-natal day 1 (P1) Sprague Dawley rats and used for explants or enzymatically dissociated and plated in dishes or in compartmentalized chambers, as previously described (Riccio et al., 1997). Explants were cultured on poly(D)lysine-laminin for 9-10 days before surgical removal of cell bodies. For cordycepin experiments, explants were treated with pentostatin (1μM for 30 min) (Chen et al., 2008), then cell bodies were removed and axons were treated with cordycepin (2.5μM for 2.5 hrs) before harvesting.

PC12 cells (purchased from ATCC) were maintained in DMEM containing 10% FBS, 5% HS (Hyclone), 2mM glutamine. To induce cell differentiation serum concentration was reduced to 0.5% FBS and 0.25% HS and NGF (50ng/mL) was added for the indicated time. Cells were transfected with Lipofectamine2000 in OptiMEM according to the manufacturer's instructions.

RNA isolation, reverse transcription, linear amplification and 3'end-RNASeq

To ensure that the axons were free of cell bodies, prior to each experiment axon compartments were incubated with Hoechst 33342 (10μg/mL in PBS for 20 min at 37˚C) and observed under an inverted fluorescent microscope. Cultures showing cell nuclei in the axon compartments or leakage of the dye in the central compartment were discarded. Total axonal and cell bodies RNA was purified from the lateral compartments of 52 or 36 chambers and the central compartment of 7 or 6 chambers respectively obtained from 3

or more independent cultures. Total RNA was isolated using PureLink® RNA Micro Scale Kit, according to the manufacturer's instructions with minor modifications. Briefly, axons and cell bodies were collected from chambers using lysis buffer (300μl) containing 10% β–mercaptoethanol. Total mRNA bound to the columns was washed and eluted twice in elution buffer (12μl). Aliquots of each sample was reverse transcribed in a 20μL reaction volume containing random hexamer mix and 50U SuperScript III Reverse Transcriptase at 50°C for 1 hr. To check the quality of samples and the absence of cell bodies contamination in axon samples, first-strand cDNAs (5μL) were PCR amplified in a 25μL PCR reaction containing actin beta or histone H4 specific primers (0.20μM), dNTPs (200 nM) and Go Taq polymerase (1.25U, Promega). Primer sequences and PCR conditions are provided (**Table S4**).

For mRNA linear amplification, samples were purified as described above, concentrated by speed-vacuum centrifugation to 1μL (axons) or 5μL (cell bodies) volume, and used for two rounds of linear amplification as previously described (Baugh et al., 2001). The volume of the first-strand reaction for the axons was scaled down to 5μL. After the second round of amplification contaminant cDNA was digested by treating the samples with RNAse-free DNAse (2U, Epicentre). Performance of the samples was tested by RT-PCR. Linear amplified aRNA from cell bodies and axon samples (2 biological replicates each) was used to prepare RNASeq libraries using the strand-specific ScriptSeq protocol (Illumina). Paired-end sequencing (2x 150bp) of four indexed libraries was performed on the Illumina HiSeq2000 platform, generating in excess of 80M mappable reads per sample. Library preparation and sequencing were performed at the Liverpool Centre for Genomic Research (CGR, http://www.liv.ac.uk/genomic-research/). Statistics of the sequencing are shown in **Table S5**.

Inference of 3'UTR isoforms from 3'-end RNA-seq

Paired-end stranded RNA-seq reads of 150 bp were mapped to the reference rat genome (UCSC, rn5) using TopHat2 (Kim et al., 2013) allowing up to 20 multi-alignments and 2 read mismatches. Nucleotide-level stranded coverage was obtained for axons and cell body samples using genomecov from the BEDTools suite (Quinlan, 2014; Quinlan and Hall, 2010). Continuously transcribed regions were identified using a sliding window across the genome requiring a minimum coverage of 7 reads in more than 80 positions per window of 100 bp; neighbouring regions separated by low-mappable regions were merged as described in (Miura et al., 2013). Expressed fragments were associated with matching strand overlapping 3'UTR using Ensembl Rn5 version 78 (v78) (Flicek et al., 2013). Isolated expressed fragments that did not overlap with any feature were associated with the closest 3'UTR if (1) the 3'UTR was <10kb and (2) there were no intervening annotations. We filtered assigned expressed fragments to exclude potential intragenic transcription, overlapping transcripts, and retained introns as described in (Miura et al., 2013). If the expressed fragment continued beyond the end of the annotated 3'UTR, we took the fragment as the new 3' end. A marked change in the level of coverage in the 3' to 5' end direction is expected to occur at the boundaries of alternative polyadenylation sites due to the accumulation of the reads in 3' termini of the transcripts. To identify alternative 3'UTR isoforms we used Segmentor3IsBack R package (Cleynen et al., 2014) that modelled nucleotide level read coverage along 3'UTRs with a negative binomial distribution and identified segments of spatially coherent coverage along individual 3'UTRs. Prior to coverage segmentation, nucleotide-level read coverage was smoothed using a running median of width 150 nts. As previously reported, each 3' end can have multiple cleavage positions in a small window (Tian et al., 2005); we thus clustered together change-points located within 25nt from one another and selected the most promoter-distal change-point. We applied the algorithm to the raw coverage and log2-scaled coverage of both cell body and axon-derived samples. We then merged all 4

annotations (cell body and axon samples, linear and log scale) and clustered 3' end located within 50 nts distance, selecting the most promoter-distal annotation. We searched the -50 nts to +150 nts region surrounding the 3' end termini of Ensembl annotated and newly annotated 3'UTR isoforms for 12 canonical and non-canonical PAS motifs listed in PolyA_db (Lee et al., 2007) (AATACA, ATTAAA, TATAAA, AATATA, AATAGA, AGTAAA, AATGAA, ACTAAA, CATAAA, GATAAA, AAGAAA, and AATAAA) using the matchPattern function from the Biostrings R package (Pages et al, 2008.). We tested for the statistical enrichment of the PAS motifs in 3'UTR isoforms using the Fisher's exact test. A polyadenylation sites atlas was combined from the following sources: 1) poly(A) site annotation (Gruber et al., 2016) build using 3'-end sequencing libraries in human and mouse, lifted from hg19/mm10 to Rn5 using python library CrossMap (Zhao et al., 2014); 2) 3'-end sequencing libraries from rat brain and testes (Derti et al., 2012); 3) 3'end annotation in Ensembl Rn6, RefSeq Rn5 and Rn6, and XenoRefSeq; 4) polyadenylation sites annotations from PolA_DB (Lee et al., 2007) and APADB (Muller et al., 2014). We next compared the percentage of newly annotated 3' ends recovered from each source and from the compiled polyadenylation site atlas at several intervals from novel 3' ends.

3'UTR isoform quantification and identification of transcripts localized to axons

The number of reads mapped to -500 nts terminal region of each 3'UTR isoform was used to calculate the expression levels. The density of mapped reads in -500 nts terminal region of 3'UTR isoforms is bimodal, with a low-density peak probably corresponding to background transcription, i.e. 3'UTR isoforms of low abundance or 3'UTR isoforms to which reads were spuriously mapped, and a high-density peak corresponding to expressed 3'UTR isoforms. In order to identify 3'UTR isoforms expressed in axons and cell body, a two-component Gaussian mixture was fitted to the data using the R package mclust (Fraley et al, 2012). An isoform was called expressed if in both replicates there

were less than 5% chance of belonging to the background category or if in at least one replicate there was more than 10% chance of belonging to the expressed category.

Differential 3'UTR isoforms expression analysis

We focused the analysis on 4,191 tandem pairs of 3'UTR isoforms expressed in the cell body and/or in axonal samples. To identify transcripts displaying a change in the 3'UTR isoform usage between axon and cell body samples, we scored the differences in promoter-proximal to promoter-distal poly(A) site usage:

$$S_1 = log_2\left(\frac{I_{proximal}}{I_{distal}}\right)_{CB} - log_2\left(\frac{I_{proximal}}{I_{distal}}\right)_{Axons}$$

$$S_2 = \frac{I_{proximal}}{I_{proximal} + I_{distal}}_{CB} - \frac{I_{proximal}}{I_{proximal} + I_{distal}}_{Axons} \in [-1,1]$$

The statistical significance of the changes in proximal-to-distal poly(A) site ratio between cell body and axons was assessed by Fisher's exact count test using summed-up raw read counts of promoter-proximal *versus* promoter-distal 3'UTR isoforms originating in the cell body or axonal samples. We applied a False Discovery Rate adjusted threshold of 0.01. A shift towards the usage of promoter-proximal isoforms in axons compared to cell body was considered when $S_1 \leq -1$, $S_2 \leq -15\%$ and FDR<0.01. A shift towards the usage of promoter-distal isoforms in axons compared to cell body was considered when $S_1 \geq 1$, $S_2 \geq 15\%$ and FDR<0.01. Finally, a stringent threshold was applied to identify highly enriched isoforms in axons as following: for those tandem 3'UTR isoforms showing shift towards the usage of promoter-proximal isoforms in axons as compared to cell body, we required $\frac{I_{proximal}}{I_{proximal}+I_{distal}}_{CB} \leq 0.2$. Conversely for those tandem 3'UTR isoforms showing shift towards the usage of promoter-distal isoforms in axons, we required $\frac{I_{proximal}}{I_{proximal}+I_{distal}}_{CB} \geq 0.8$.

Gene Ontology enrichment analysis

GO analysis was performed by comparing pairs of gene lists using the Fisher test with the topGO Bioconductor package (Alexa and Rahnenfuhrer, 2016). Only GO terms containing at least 10 annotated genes were considered. We applied a P-value threshold of 0.05. We manually filtered biologically relevant and statistically enriched GO by removing redundant GO terms and those applying to fewer than 5 genes in the gene lists.

RT-PCR and quantitative RT-PCR

mRNA was isolated from sympathetic neurons or PC12 cells using TRIzol or RNAEasy mini Kit (QIAGEN) and reverse transcribed. qRT-PCR reactions (20μL) contained 10μL of Flash SybrGreen Mastermix, or 12.5μL of SybrSelect Mastermix and 0.25μM primers, unless otherwise indicated. Reactions were performed in duplicate or triplicate with the Mastercycler® ep realplex qPCR machine (Eppendorf). For absolute quantification, each experiment included a standard curve, a no-RT control and a no-template control. Standard templates consisted of gel-purified PCR amplicons of known concentrations and each standard curve consisted of seven serial dilutions of the DNA template. For relative quantification, the Comparative Ct Method (ΔΔCt Method) was used. At the end of 40 cycles of amplification, a dissociation curve was performed in which SybrGreen fluorescence was measured at 1ºC intervals between the annealing temperature and 100ºC. Melting temperatures of amplicons varied between 80°C and 92°C. Primer sequences and PCR conditions are described in **Table S4**.

Northern blotting

RNA purified from SCG neurons cultured for 7 days or PC12 cells was separated by electrophoresis in denaturing conditions and transferred to nylon membrane by capillary blotting according to standard protocols. Probes corresponding to *IMPA1, Firefly Luciferase* or *GAPDH* coding sequences, or *IMPA1L* 120nt fragment were labeled using

Random priming Labeling Kits (Takara or Roche) and [α–^{32}P] dCTP. Blots were exposed to films or phosphorimager screens. Radioactive signal was quantified using ImageQuant TL software (GE Healthcare).

Tag Addition-PolyAdenylation Test (TA-PAT)

The PAT assay was performed as described (di Penta et al., 2009) with minor modifications. Briefly, total RNA was purified from PC12 cells, tagged by annealing the TA-PAT template1 primer to the end of the mRNA, and extended with Klenow polymerase (NEB, 37°C for 60min). The tagged RNA was reverse transcribed by Superscript™ III Reverse Transcriptase (42°C for 60min) using the TA-PAT RT primer 1 and cDNA was amplified using the IMPA1-1351 forward primer that anneals just upstream of the IMPA1-SS poly(A) and the TA-PAT RT primer 1 as reverse primer. Primer sequences and PCR conditions are described in **Table S4**.

3' rapid amplification of cDNA ends (3' RACE)

Full length 3'UTR of *IMPA1*, *actin beta*, *stathmin 2* and *cofilin1* mRNAs were amplified from axonal and cell body compartments by performing 3' RACE reactions on total RNA isolated from compartmentalized chambers as previously described (Andreassi et al., 2010). Samples were concentrated by speed-vacuum, RNA was divided in two equal samples and used for amplification with SMART RACE cDNA Amplification Kit (Clontech) according to manufacturer's instructions. Gene specific primers for 3' RACE assays are listed in **Table S4**. Amplification was performed using Advantage GC 2 PCR kit (Clontech) and PCR products were cloned and sequenced.

Cloning

IMPA1 Super-Short (*IMPA1-SS*) and *Long* (*IMPA1-L*) 3'UTR sequences were amplified by PCR from the corresponding RACE clones. After digestion with *NotI*/*XhoI*, IMPA1-SS DNA fragment was purified and used to replace IMPA1-L in myrdEGFP-IMPA1-L (Andreassi et al., 2010). Mouse IMPA1 coding sequence was PCR-amplified from mouse

brain cDNA using primers encoding the HA tag. After digestion with *Bam*HI/*NotI*, *ms* HA-IMPA1 DNA fragments were purified and used to replace dEGFP sequence in myrdEGFP-IMPA1-L or myrdEGFP-IMPA1-SS. The 120 nts localization signal of IMPA1-L was cloned by PCR from a *IMPA1-L* RACE clone and cloned at the 3' of *ms* HA-IMPA1-*rat* SS plasmid. To generate Firefly IMPA1-SS, -L or –LΔpoly(A) vectors, *Firefly luciferase* coding sequence was PCR amplified from pGL3 vector (Promega) with primers containing restriction sites for *Bam*HI and *NotI*. The DNA fragment was purified and used to replace the myrdEGFP sequence in myrdEGFP-IMPA1-SS or myrdEGFP-IMPA1-L. Mutation of IMPA1-SS and IMPA-1S poly(A) sites was performed by PCR site-directed mutagenesis (Agilent) of Firefly-IMPA1-L vector. In all Firefly constructs, the bovine Growth Hormone poly(A) sequence was removed by PCR site-directed mutagenesis to create an extra *XhoI* site, that was used for digestion and re-ligation. Primer sequences and PCR conditions are described in **Table S4**.

Electroporation and analysis of mRNA transport in axons

Neurons were electroporated with the indicated constructs as previously described (http://www.cellectricon.se/pdf/Sympathetic_neurons.pdf). MyrdEGFP was detected by GFP immunostaining. Confocal images were acquired with a SP5 confocal system (Leica) using LAS AF software and automated tiling over several z-stacks, to cover the whole thickness and length of the axons. Maximal intensity projections were processed with Fiji software. Axons were traced manually using NeuronJ plugin and grey value intensity over length was measured. Data analysis was performed using Excel software to calculate average values and standard error means of the intensity for each 100μm axonal segment.

Quantification of axon degeneration

SGC explants were grown for 36 hours before electroporation with the indicated siRNAs (150nM, GE Dharmacon) and a GFP expression vector (20ng/μL), in the presence of

either *ms* HA-IMPA1-rat SS, *ms* HA-IMPA1-rat SS+120, or *m s*HA-IMPA1-rat L DNAs, (200 ng/μL), as indicated. After 6 days, GFP fluorescence was detected with an inverted Leica epifluorescence microscope, and intact axon bundles that showed no sign of breakdown were quantified. For imaging, explants were fixed in 4% PFA and stained with anti-GFP and anti-neurofilament antibodies. Antibodies and probing conditions are described in **Table S4**.

Co-immunoprecipitation and western blotting

Co-immunoprecipitation samples were obtained by lysing cells in RIPA buffer (50 mM Tris-HCl pH 7.4, 150 mM NaCl, 1% NP-40, 0.5% Sodium deoxycholate, 0.1% SDS, 1 mM EDTA, Protease Inhibitors Cocktail) for 10min on ice. After centrifugation, protein concentration in the supernatants was assayed by Pierce™ BCA Assay, and 0.5-1 mg of pre-cleared protein sample was incubated with 2μg of antibody as indicated, overnight at 4ºC, on constant rotation. Immuno-complexes were precipitated by adding protein A-agarose beads (GE Healthcare) at 4ºC for 2hrs. After extensive washes with RIPA buffer, immunocomplexes were eluted from the beads by boiling in 1X LDS-buffer +2.5% βmercaptoethanol. Samples were resolved on 4-12% PAA pre-cast gels and blotted on PVDF membrane (Amersham). For western blotting, cells were rinsed with PBS and lysed in the plates with 1X LDS-buffer +10% βmercaptoethanol. SDS-PAGE and blotting was then performed as described above. For immunodetection, membranes were blocked in 5% milk for 1hr at room temperature and incubated overnight with the indicated antibodies. Antibodies and probing conditions are shown in **Table S4**.

RNA ImmunoPrecipitation (RIP)

RNA immunoprecipitation was performed as described (Napoli et al., 2008) with minor modifications. Briefly, protein A/G agarose beads (Santa Cruz) were incubated with antibody (5μg in 1% BSA in PBS) and heparin (1mg/ml) for 2hrs at 4ºC, washed with

washing buffer (150mM NaCl, 50mM Tris-HCl [pH 8.0], 1% Triton X-100), and incubated with 250-300μg of protein lysates 1 hr at 4ºC. Beads were extensively washed, and RNA was eluted in 0.2M Na Acetate, 1mM EDTA, and 0.2% SDS for 5 min at 70ºC. For normalization, 20pg of *in vitro* transcribed RNA synthesized from the T7 control DNA Template (AmpliScribe™ T7 Transcription Kit, Epicentre) was added to the samples. RNA from inputs and immunocomplexes was purified, subjected to DNAse digestion (Ambion), reverse transcribed and assayed by qPCR. Primer sequences and PCR conditions are described in **Table S4**.

Dual luciferase assay

PC12 cells were transfected with the indicated *Firefly* Luciferase-IMPA1 constructs and thymidine-kinase – *Renilla* Luciferase (Promega) using Lipofectamine 2000 for 48hrs. Samples were processed using the dual-luciferase reporter assay system (Promega), according to manufacturer's instructions.

Polysomal fractionation

Polysomal fractionation was performed as described (Johannes and Sarnow, 1998). Briefly, PC12 cells were lysed in ice-cold gradient buffer (0.3M NaCl, 1mM $MgCl_2$, 15mM Tris-HCl (PH7.4), 0.1mg/mL cyclohexamide and 1mg/mL heparin, 1% Triton X-100, 500U/mL RNAse inhibitors). Samples were centrifuged and the supernatants layered onto 10–50% sucrose linear gradients. The gradients were sedimented at 38,000 r.p.m., using a SW40Ti rotor (Beckman) or a Sorvall TH-641 rotor for 2 hrs at 4°C. Eleven fractions (1mL each) were collected from the gradients and transferred in 3ml of 7.7M guanidine-HCL using a Foxy R1 gradient fractionator (Teledyne ISCO; ISCO peak Trak version 1.10 software) with continuous measurement of the absorbance at 254nm. RNA was precipitated, treated with DNAse and purified using RNAeasy Mini Kit (QIAGEN). For fractions 1 and 2, protocol was modified as suggested by manufacturer for recovery of

small size RNA. Samples were concentrated by speed-vacuum and analysed by northern blot.

Mass-spectrometry

Immuno-complexes were precipitated from $20x10^6$ PC12 cells naïve or differentiated with NGF for 4 days. On-bead digestion and nano LC-MS/MS analysis was performed as described (Bernaudo et al., 2015) with minor changes. The procedure is summarized in **Figure S5**, and described briefly below. Immuno-precipitated proteins were released from the resin by on-beads digestion for 15min at 37°C using 200ng of trypsin (Promega). The supernatants were collected and subjected to conventional in-solution tryptic digestion (overnight at 37ºC) in denaturing conditions (reduction by 10mM DTT for 1hr at 37ºC followed by 24mM iodoacetamide for 1hr at 37ºC quenched by addition of 2mM DTT for 30min at 37ºC). Tryptic peptides were then subjected to differential labelling by either oxygen[18] or dimethyl labelling (Boersema et al., 2009). Pairs of differently labelled samples were mixed, purified by StageTips (Rappsilber et al., 2007) and subjected to nano LC-MS/MS analysis. Chromatography was performed on an Easy LC 1000 nanoLC system (Thermo Fisher Scientific, Odense, Denmark). The analytical nanoLC column was a pulled fused silica capillary, 75µm i.d., in-house packed to a length of 10 cm with 3µm C18 silica particles from Dr. Maisch GmbH (Entringen, Germany). A 60-min binary gradient was used for peptide elution. MS detection was performed on a quadruple-orbitrap mass spectrometer Q-Exactive (Thermo Fisher Scientific) operating in positive ion mode and data-dependent (Top-12) scanning mode. Data were processed using Proteome Discoverer 1.4 (Thermo Fisher Scientific), using Sequest as search engine, and querying the March 2015 RATTUS reference proteome sequence database (http://www.ebi.ac.uk/uniprot). The protein sequence database was merged with a list of common contaminants named “Common Repository of Adventitious Proteins” retrieved from The Global Proteome Machine website (http://www.thegpm.org/crap/index.html). In

total, 27,927 entries were searched. Peptide identifications were validated by Percolator (Kall et al., 2007) integrated in Proteome Discoverer. Percolator q-value was set to equal or less than 0.05. Quantification values based on < 3 peptides were manually checked in raw MS data. MS/MS data relative to protein hits identified by a single peptide are reported in **Table S5**. Protein H:L ratios obtained from all technical replicates of a given biological replicate were transformed into $\log_2$ space before their median was calculated.

RNA oligo-Mediated Ligation (RML) RT-PCR

RML RT-PCR was performed as described (Endres et al., 2011) with the following modifications. Cleaved fragments were isolated and cloned using 1.2ng of axonal RNA purified and pooled from 55 explants where the cell bodies had been surgically removed, or 1.5 μg or less of total cellular RNA. Total cellular RNA was DNAse-digested and purified by phenol:chloroform purification. Quality control of starting material was performed using Agilent Tapestation 2200 (UCL Genomics). Samples with a RIN value≥ 7.2 were used for RLM RT-PCR. RNA was denatured and tagged by ligation with 25ng or 250ng for axonal or total RNA, of RNA oligo and 30U of T_4 RNA ligase (NEB) for 1hr at 37ºC followed by overnight incubation at 16ºC in a PCR machine. Ligated axonal RNA was then purified using buffer PB+10% β–mercaptoethanol (QIAGEN) and AMPure XP beads (Beckman Coulter) as per manufacturer's instructions. Total RNA was purified as described above. Ligated RNA was reverse transcribed using random hexamers and 50U SuperScript IV reverse transcriptase (Thermo Fisher Scientific) for 1hr at 50ºC. After RNAseH digestion, cleaved fragments were amplified by PCR using Q5 DNA polymerase (NEB) and cloned in pCR™4Blunt-TOPO® vector according to manufacturer's instruction. At least 15 individual, random clones were analyzed by sequencing. When used for RT-qPCR, amplification of the cleaved fragments was carried out in 25μL reaction using SybrSelect MasterMix. Primer sequences and PCR conditions are described in **Table S4**.

Statistical analyses

Data are expressed as averages ± SEM. One-way ANOVA with post-hoc test or t-test were used as indicated to test for statistical significance, which was placed at $P < 0.05$ unless otherwise noted.

Accession numbers

The RNA-seq data and the new 3'UTR annotation will be available at Gene Expression Omnibus; the accession number is in preparation. The source code will available at Githb.

AUTHOR CONTRIBUTION

CA conceived the project and performed most experiments. RL and NL performed the bioinformatics analysis. HC performed the co-immunoprecipitations and helped with the cell cultures and the biochemistry experiments. SF performed RIP experiments. MG and GC performed the mass spectrometry and analysed the data. AR conceived the project and wrote the manuscript, which included suggestions from all authors.

ACKNOWLEDGEMENTS

We thank Cristina Ottone for generating the Firefly-IMPA1 3'UTRs constructs, and Carola Zimmermann for sharing the drawing and the staining of compartmentalized chambers, and for performing the Stahmin2 RACE shown in **Fig.1I**. We are indebted to Anne Willis and the Genomic Service (University of Leicester) for the use of the Foxy R1 gradient fractionator and to Tina Daviter (ISMB Biophysics Centre at Birkbeck, University of London) for the use of the phosphorimager. We thank Adolfo Saiardi, Paolo Salomoni and Jernej Ule for insightful suggestions on the manuscript, and all members of the Riccio lab for helpful discussions. This work was supported by the Wellcome Trust Investigator Award 103717/Z/14/Z (to A.R.), an MRC Senior Non Clinical Fellowship SNCF G0802010 (to A.R.), the MRC LMCB Core Grant MC_U12266B, a Wellcome Trust Institutional Strategic Support Fund 2014 (to C.A.), an Early Postdoc Mobility fellowship from the Swiss National Science Foundation P2BSP3_158800 (to R.L.) and a Marie Curie Post-doctoral Research Fellowship 657749-NeuroUTR (to R.L.) and a MIUR, Programma Operativo Nazionale, iCARE project, grant no. ICARE PON03PE_0009_2 (to M.G.).

REFERENCES

Aakalu, G., Smith, W.B., Nguyen, N., Jiang, C., and Schuman, E.M. (2001). Dynamic visualization of local protein synthesis in hippocampal neurons. Neuron *30*, 489-502.

Allen, M., Bird, C., Feng, W., Liu, G., Li, W., Perrone-Bizzozero, N.I., and Feng, Y. (2013). HuD promotes BDNF expression in brain neurons via selective stabilization of the BDNF long 3'UTR mRNA. PloS one *8*, e55718.

An, J.J., Gharami, K., Liao, G.Y., Woo, N.H., Lau, A.G., Vanevski, F., Torre, E.R., Jones, K.R., Feng, Y., Lu, B.*, et al.* (2008). Distinct role of long 3' UTR BDNF mRNA in spine morphology and synaptic plasticity in hippocampal neurons. Cell *134*, 175-187.

Andreassi, C., and Riccio, A. (2009). To localize or not to localize: mRNA fate is in 3'UTR ends. Trends in cell biology *19*, 465-474.

Andreassi, C., Zimmermann, C., Mitter, R., Fusco, S., De Vita, S., Saiardi, A., and Riccio, A. (2010). An NGF-responsive element targets myo-inositol monophosphatase-1 mRNA to sympathetic neuron axons. Nature neuroscience *13*, 291-301.

Baleriola, J., Walker, C.A., Jean, Y.Y., Crary, J.F., Troy, C.M., Nagy, P.L., and Hengst, U. (2014). Axonally synthesized ATF4 transmits a neurodegenerative signal across brain regions. Cell *158*, 1159-1172.

Baugh, L.R., Hill, A.A., Brown, E.L., and Hunter, C.P. (2001). Quantitative analysis of mRNA amplification by in vitro transcription. Nucleic acids research *29*, E29.

Ben-Yaakov, K., Dagan, S.Y., Segal-Ruder, Y., Shalem, O., Vuppalanchi, D., Willis, D.E., Yudin, D., Rishal, I., Rother, F., Bader, M.*, et al.* (2012). Axonal transcription factors signal retrogradely in lesioned peripheral nerve. The EMBO journal *31*, 1350-1363.

Bernaudo, F., Monteleone, F., Mesuraca, M., Krishnan, S., Chiarella, E., Scicchitano, S., Cuda, G., Morrone, G., Bond, H.M., and Gaspari, M. (2015). Validation of a novel shotgun proteomic workflow for the discovery of protein-protein interactions: focus on ZNF521. Journal of proteome research *14*, 1888-1899.

Boersema, P.J., Raijmakers, R., Lemeer, S., Mohammed, S., and Heck, A.J. (2009). Multiplex peptide stable isotope dimethyl labeling for quantitative proteomics. Nature protocols *4*, 484-494.

Chen, L.S., Stellrecht, C.M., and Gandhi, V. (2008). RNA-directed agent, cordycepin, induces cell death in multiple myeloma cells. British journal of haematology *140*, 682-391.

Cleynen, A., Koskas, M., Lebarbier, E., Rigaill, G., and Robin, S. (2014). Segmentor3IsBack: an R package for the fast and exact segmentation of Seq-data. Algorithms for molecular biology : AMB *9*, 6.

Colak, D., Ji, S.J., Porse, B.T., and Jaffrey, S.R. (2013). Regulation of axon guidance by compartmentalized nonsense-mediated mRNA decay. Cell *153*, 1252-1265.

Cosker, K.E., Fenstermacher, S.J., Pazyra-Murphy, M.F., Elliott, H.L., and Segal, R.A. (2016). The RNA-binding protein SFPQ orchestrates an RNA regulon to promote axon viability. Nature neuroscience *19*, 690-696.

Derti, A., Garrett-Engele, P., Macisaac, K.D., Stevens, R.C., Sriram, S., Chen, R., Rohl, C.A., Johnson, J.M., and Babak, T. (2012). A quantitative atlas of polyadenylation in five mammals. Genome research *22*, 1173-1183.

di Penta, A., Mercaldo, V., Florenzano, F., Munck, S., Ciotti, M.T., Zalfa, F., Mercanti, D., Molinari, M., Bagni, C., and Achsel, T. (2009). Dendritic LSm1/CBP80-mRNPs mark the early steps of transport commitment and translational control. The Journal of cell biology *184*, 423-435.

Endres, M.W., Cook, R.T., and Gregory, B.D. (2011). A high-throughput sequencing-based methodology to identify all uncapped and cleaved RNA molecules in eukaryotic genomes. Methods in molecular biology *732*, 209-223.

Eom, T., Antar, L.N., Singer, R.H., and Bassell, G.J. (2003). Localization of a beta-actin messenger ribonucleoprotein complex with zipcode-binding protein modulates the density

of dendritic filopodia and filopodial synapses. The Journal of neuroscience : the official journal of the Society for Neuroscience *23*, 10433-10444.

Flavell, S.W., Kim, T.K., Gray, J.M., Harmin, D.A., Hemberg, M., Hong, E.J., Markenscoff-Papadimitriou, E., Bear, D.M., and Greenberg, M.E. (2008). Genome-wide analysis of MEF2 transcriptional program reveals synaptic target genes and neuronal activity-dependent polyadenylation site selection. Neuron *60*, 1022-1038.

Flicek, P., Ahmed, I., Amode, M.R., Barrell, D., Beal, K., Brent, S., Carvalho-Silva, D., Clapham, P., Coates, G., Fairley, S.*, et al.* (2013). Ensembl 2013. Nucleic acids research *41*, D48-55.

Gruber, A.J., Schmidt, R., Gruber, A.R., Martin, G., Ghosh, S., Belmadani, M., Keller, W., and Zavolan, M. (2016). A comprehensive analysis of 3' end sequencing data sets reveals novel polyadenylation signals and the repressive role of heterogeneous ribonucleoprotein C on cleavage and polyadenylation. Genome research *26*, 1145-1159.

Hinnebusch, A.G., Ivanov, I.P., and Sonenberg, N. (2016). Translational control by 5'-untranslated regions of eukaryotic mRNAs. Science *352*, 1413-1416.

Hogg, J.R., and Goff, S.P. (2010). Upf1 senses 3'UTR length to potentiate mRNA decay. Cell *143*, 379-389.

Holt, C.E., and Schuman, E.M. (2013). The central dogma decentralized: new perspectives on RNA function and local translation in neurons. Neuron *80*, 648-657.

Hurt, J.A., Robertson, A.D., and Burge, C.B. (2013). Global analyses of UPF1 binding and function reveal expanded scope of nonsense-mediated mRNA decay. Genome research *23*, 1636-1650.

Jalkanen, A.L., Coleman, S.J., and Wilusz, J. (2014). Determinants and implications of mRNA poly(A) tail size--does this protein make my tail look big? Seminars in cell & developmental biology *34*, 24-32.

Johannes, G., and Sarnow, P. (1998). Cap-independent polysomal association of natural mRNAs encoding c-myc, BiP, and eIF4G conferred by internal ribosome entry sites. Rna *4*, 1500-1513.

Kall, L., Canterbury, J.D., Weston, J., Noble, W.S., and MacCoss, M.J. (2007). Semi-supervised learning for peptide identification from shotgun proteomics datasets. Nature methods *4*, 923-925.

Karginov, F.V., Cheloufi, S., Chong, M.M., Stark, A., Smith, A.D., and Hannon, G.J. (2010). Diverse endonucleolytic cleavage sites in the mammalian transcriptome depend upon microRNAs, Drosha, and additional nucleases. Molecular cell *38*, 781-788.

Kim, D., Pertea, G., Trapnell, C., Pimentel, H., Kelley, R., and Salzberg, S.L. (2013). TopHat2: accurate alignment of transcriptomes in the presence of insertions, deletions and gene fusions. Genome biology *14*, R36.

Kislauskis, E.H., Zhu, X., and Singer, R.H. (1994). Sequences responsible for intracellular localization of beta-actin messenger RNA also affect cell phenotype. The Journal of cell biology *127*, 441-451.

Kocabas, A., Duarte, T., Kumar, S., and Hynes, M.A. (2015). Widespread Differential Expression of Coding Region and 3' UTR Sequences in Neurons and Other Tissues. Neuron *88*, 1149-1156.

Kurosaki, T., and Maquat, L.E. (2013). Rules that govern UPF1 binding to mRNA 3' UTRs. Proceedings of the National Academy of Sciences of the United States of America *110*, 3357-3362.

Lee, J.Y., Yeh, I., Park, J.Y., and Tian, B. (2007). PolyA_DB 2: mRNA polyadenylation sites in vertebrate genes. Nucleic acids research *35*, D165-168.

Leung, K.M., van Horck, F.P., Lin, A.C., Allison, R., Standart, N., and Holt, C.E. (2006). Asymmetrical beta-actin mRNA translation in growth cones mediates attractive turning to netrin-1. Nature neuroscience *9*, 1247-1256.

Lianoglou, S., Garg, V., Yang, J.L., Leslie, C.S., and Mayr, C. (2013). Ubiquitously transcribed genes use alternative polyadenylation to achieve tissue-specific expression. Genes & development *27*, 2380-2396.

Martin, K.C., and Ephrussi, A. (2009). mRNA localization: gene expression in the spatial dimension. Cell *136*, 719-730.

Mercer, T.R., Wilhelm, D., Dinger, M.E., Solda, G., Korbie, D.J., Glazov, E.A., Truong, V., Schwenke, M., Simons, C., Matthaei, K.I.*, et al.* (2011). Expression of distinct RNAs from 3' untranslated regions. Nucleic acids research *39*, 2393-2403.

Miura, P., Shenker, S., Andreu-Agullo, C., Westholm, J.O., and Lai, E.C. (2013). Widespread and extensive lengthening of 3' UTRs in the mammalian brain. Genome research *23*, 812-825.

Muller, S., Rycak, L., Afonso-Grunz, F., Winter, P., Zawada, A.M., Damrath, E., Scheider, J., Schmah, J., Koch, I., Kahl, G.*, et al.* (2014). APADB: a database for alternative polyadenylation and microRNA regulation events. Database : the journal of biological databases and curation *2014*.

Napoli, I., Mercaldo, V., Boyl, P.P., Eleuteri, B., Zalfa, F., De Rubeis, S., Di Marino, D., Mohr, E., Massimi, M., Falconi, M.*, et al.* (2008). The fragile X syndrome protein represses activity-dependent translation through CYFIP1, a new 4E-BP. Cell *134*, 1042-1054.

Nicholson, P., Yepiskoposyan, H., Metze, S., Zamudio Orozco, R., Kleinschmidt, N., and Muhlemann, O. (2010). Nonsense-mediated mRNA decay in human cells: mechanistic insights, functions beyond quality control and the double-life of NMD factors. Cellular and molecular life sciences : CMLS *67*, 677-700.

Pai, A.A., Baharian, G., Page Sabourin, A., Brinkworth, J.F., Nedelec, Y., Foley, J.W., Grenier, J.C., Siddle, K.J., Dumaine, A., Yotova, V.*, et al.* (2016). Widespread Shortening of 3' Untranslated Regions and Increased Exon Inclusion Are Evolutionarily Conserved Features of Innate Immune Responses to Infection. PLoS genetics *12*, e1006338.

Perrone-Bizzozero, N., and Bird, C.W. (2013). Role of HuD in nervous system function and pathology. Frontiers in bioscience *5*, 554-563.

Perry, R.B., Doron-Mandel, E., Iavnilovitch, E., Rishal, I., Dagan, S.Y., Tsoory, M., Coppola, G., McDonald, M.K., Gomes, C., Geschwind, D.H.*, et al.* (2012). Subcellular knockout of importin beta1 perturbs axonal retrograde signaling. Neuron *75*, 294-305.

Proudfoot, N.J. (2011). Ending the message: poly(A) signals then and now. Genes & development *25*, 1770-1782.

Quinlan, A.R. (2014). BEDTools: The Swiss-Army Tool for Genome Feature Analysis. Current protocols in bioinformatics *47*, 11 12 11-34.

Quinlan, A.R., and Hall, I.M. (2010). BEDTools: a flexible suite of utilities for comparing genomic features. Bioinformatics *26*, 841-842.

Rappsilber, J., Mann, M., and Ishihama, Y. (2007). Protocol for micro-purification, enrichment, pre-fractionation and storage of peptides for proteomics using StageTips. Nature protocols *2*, 1896-1906.

Riccio, A., Pierchala, B.A., Ciarallo, C.L., and Ginty, D.D. (1997). An NGF-TrkA-mediated retrograde signal to transcription factor CREB in sympathetic neurons. Science *277*, 1097-1100.

Sambandan, S., Akbalik, G., Kochen, L., Rinne, J., Kahlstatt, J., Glock, C., Tushev, G., Alvarez-Castelao, B., Heckel, A., and Schuman, E.M. (2017). Activity-dependent spatially localized miRNA maturation in neuronal dendrites. Science *355*, 634-637.

Sandberg, R., Neilson, J.R., Sarma, A., Sharp, P.A., and Burge, C.B. (2008). Proliferating cells express mRNAs with shortened 3' untranslated regions and fewer microRNA target sites. Science *320*, 1643-1647.

Shepard, P.J., Choi, E.A., Lu, J., Flanagan, L.A., Hertel, K.J., and Shi, Y. (2011). Complex and dynamic landscape of RNA polyadenylation revealed by PAS-Seq. Rna *17*, 761-772.

Shigeoka, T., Jung, H., Jung, J., Turner-Bridger, B., Ohk, J., Lin, J.Q., Amieux, P.S., and Holt, C.E. (2016). Dynamic Axonal Translation in Developing and Mature Visual Circuits. Cell *166*, 181-192.

Singh, G., Pratt, G., Yeo, G.W., and Moore, M.J. (2015). The Clothes Make the mRNA: Past and Present Trends in mRNP Fashion. Annual review of biochemistry *84*, 325-354.

Taliaferro, J.M., Vidaki, M., Oliveira, R., Olson, S., Zhan, L., Saxena, T., Wang, E.T., Graveley, B.R., Gertler, F.B., Swanson, M.S.*, et al.* (2016). Distal Alternative Last Exons Localize mRNAs to Neural Projections. Molecular cell *61*, 821-833.

Thomas-Jinu, S., Gordon, P.M., Fielding, T., Taylor, R., Smith, B.N., Snowden, V., Blanc, E., Vance, C., Topp, S., Wong, C.H.*, et al.* (2017). Non-nuclear Pool of Splicing Factor SFPQ Regulates Axonal Transcripts Required for Normal Motor Development. Neuron *94*, 322-336 e325.

Tian, B., Hu, J., Zhang, H., and Lutz, C.S. (2005). A large-scale analysis of mRNA polyadenylation of human and mouse genes. Nucleic acids research *33*, 201-212.

Tian, B., and Manley, J.L. (2013). Alternative cleavage and polyadenylation: the long and short of it. Trends in biochemical sciences *38*, 312-320.

Wang, W., van Niekerk, E., Willis, D.E., and Twiss, J.L. (2007). RNA transport and localized protein synthesis in neurological disorders and neural repair. Developmental neurobiology *67*, 1166-1182.

Will, T.J., Tushev, G., Kochen, L., Nassim-Assir, B., Cajigas, I.J., Tom Dieck, S., and Schuman, E.M. (2013). Deep sequencing and high-resolution imaging reveal compartment-specific localization of Bdnf mRNA in hippocampal neurons. Science signaling *6*, rs16.

Willis, D., Li, K.W., Zheng, J.Q., Chang, J.H., Smit, A.B., Kelly, T., Merianda, T.T., Sylvester, J., van Minnen, J., and Twiss, J.L. (2005). Differential transport and local translation of cytoskeletal, injury-response, and neurodegeneration protein mRNAs in

axons. The Journal of neuroscience : the official journal of the Society for Neuroscience *25*, 778-791.

Yao, J., Sasaki, Y., Wen, Z., Bassell, G.J., and Zheng, J.Q. (2006). An essential role for beta-actin mRNA localization and translation in Ca2+-dependent growth cone guidance. Nature neuroscience *9*, 1265-1273.

Zhao, H., Sun, Z., Wang, J., Huang, H., Kocher, J.P., and Wang, L. (2014). CrossMap: a versatile tool for coordinate conversion between genome assemblies. Bioinformatics *30*, 1006-1007.

Figure 1

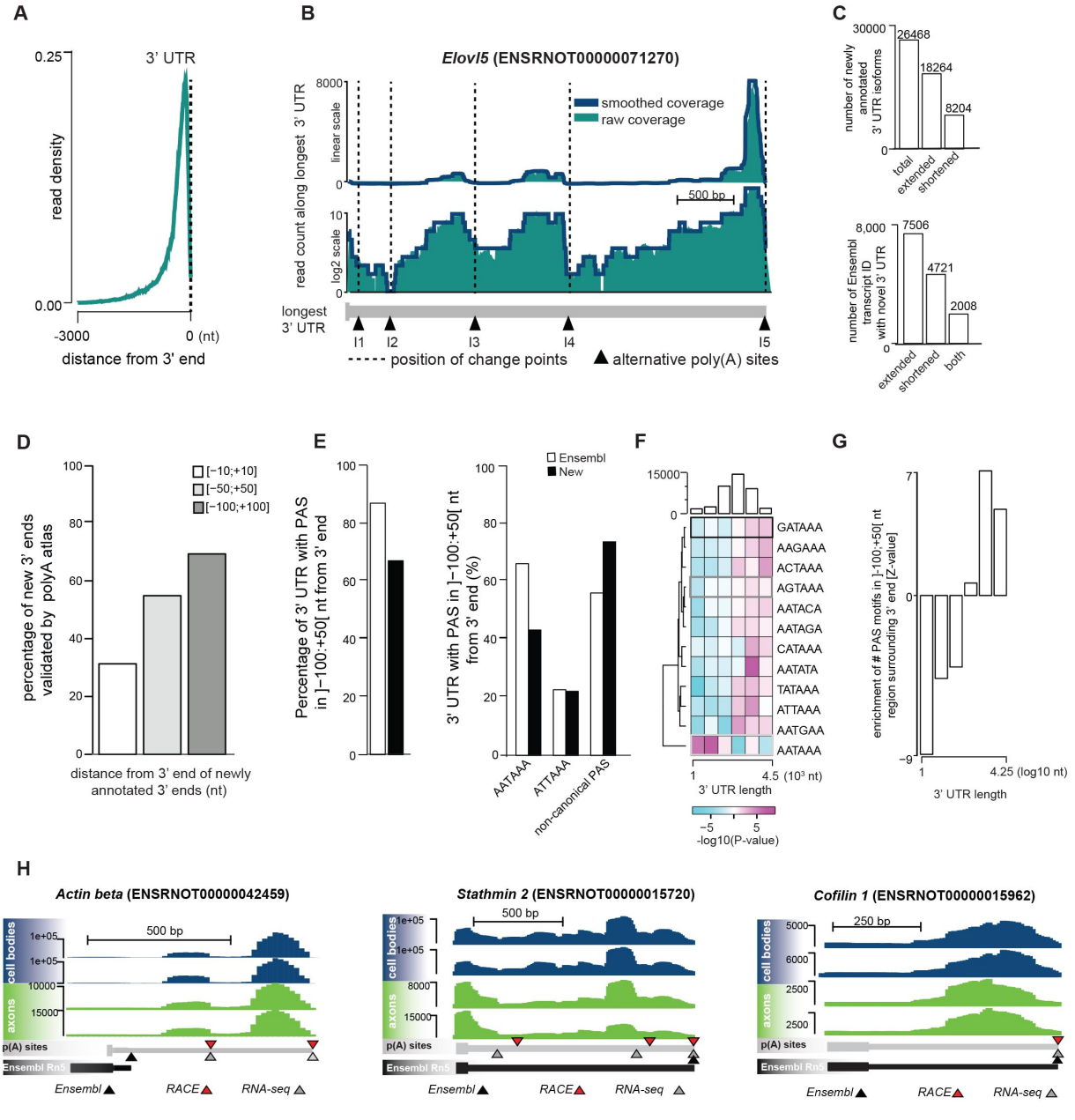

Figure 1: **3' end-RNA-seq of linearly amplified RNA from axons and cell bodies of sympathetic neurons. (A)** Accumulation of reads at the 3' end of the transcripts. The read density (number of reads per nucleotide divided by the total number of reads) of 4,975 transcripts between 2000 and 3000 nts long is shown. Dashed line indicates the 3' end. (**B**) Identification of novel 3' ends in the longest 3'UTR of *Elovl5*. Raw coverage was smoothed using a running median (window width = 100 nts) and potential 3' ends were identified by segmenting sudden transitions in read depth. (**C**) Number of newly annotated 3'UTR isoforms compared with Ensembl Rn5 annotations (*Upper panel*). Number of Ensembl transcript ID expanded with newly annotated 3'UTRs (*Lower panel*). (**D**) Percentage of newly annotated 3' ends recovered from a polyadenylation site atlas compiled from multiple sources (see Experimental Procedures) at the indicated intervals from novel 3' ends. (**E**) Frequency of canonical and variant PAS motifs detected between -100 to +50 of newly annotated (black) or Ensembl annotated (white) 3' ends. (*Left*) Total PAS motifs. (*Right*) Canonical *versus* variant PAS motifs. (**F**) Relative occurrence of different PAS motifs in promoter-proximal and promoter-distal 3'UTRs. Upper column graph indicates the number of 3'UTR isoforms per range of 3'UTR length. Colour-scale: -log10(P-value) of enrichment in PAS motif obtained by Fisher test of the number of 3' end that contains at least one motif per range of 3'UTR length. (**G**) Enrichment of the number of PAS motifs in regions surrounding 3' end with increasing 3'UTR length. (**H**) Genome browser view of the *Actin beta*, *Stathmin 2* and *Cofilin 1* 3'UTRs. 3' end isoforms annotated in Ensembl Rn5 or identified by RNA-seq data and by RACE are indicated by arrowheads. (**I**) Agarose gel analysis of RACE products to amplify *actin beta*, *Stathmin 2* and *Cofilin 1* 3'UTRs (*left panels*) and restriction digestions of representative clones obtained by cloning of corresponding RACE PCR products (*right panels*). See also **Figure S1.**

Figure 2

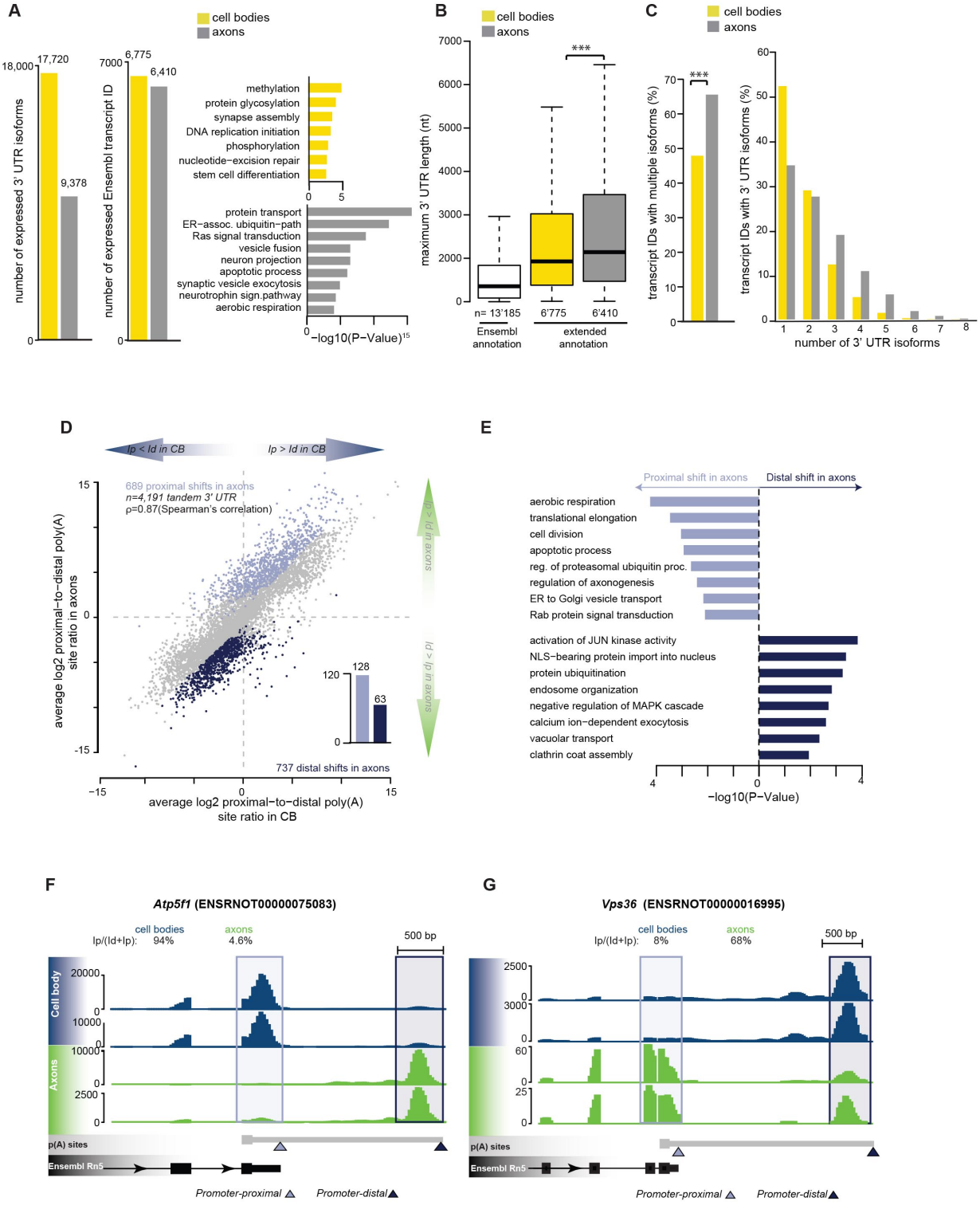

Figure 2: **Analysis of 3'UTR length and PAS choice in axonal and cell bodies transcriptomes.** (**A**) Comparative analysis of 3'UTR isoforms and transcript IDs expressed in the cell body (yellow) and axons (grey) (L*eft*). Statistically enriched GO terms of genes identified in cell bodies and axons samples *(Right*). (**B**) Maximum 3'UTR lengths for existing annotations in Ensembl Rn5 and newly identified in this study (*** $p < 0.01$; Wilcoxon rank sum test). (**C**) Percentage of cell body and axonal transcript IDs showing multiple 3'UTRs (L*eft*) and distribution of 3'UTR isoforms per expressed Ensembl transcript ID (*Right*). *** *P*-value < 0.01 (Fisher exact count test). (**D**) Scatter plot of the relative usage of promoter-proximal and promoter-distal poly(A) sites in cell bodies and axons. FDR<0.01 between cell body and axonal compartment (Fisher exact test). Dark blue = distal shifts in axons compared to cell body. Light blue = proximal shifts in axons compared to cell body. (*Inset*) 3'UTR isoforms with proximal or distal shift uniquely detected in axons when we required that usage of promoter-proximal or distal 3'UTR isoform in cell body sample was less than 20% of total isoforms. (**E**) Statistically enriched GO terms for transcripts showing a proximal (*Top*) or distal (*Bottom*) shift in poly(A) site usage in axons. (**F** and **G**) Genome browser view of representative transcripts with a marked shift towards decreased (*Atp5f1*) or increased (*Vps36*) promoter-proximal poly(A) site usage in axons compared to cell bodies. See also **Figure S2**.

Figure 3

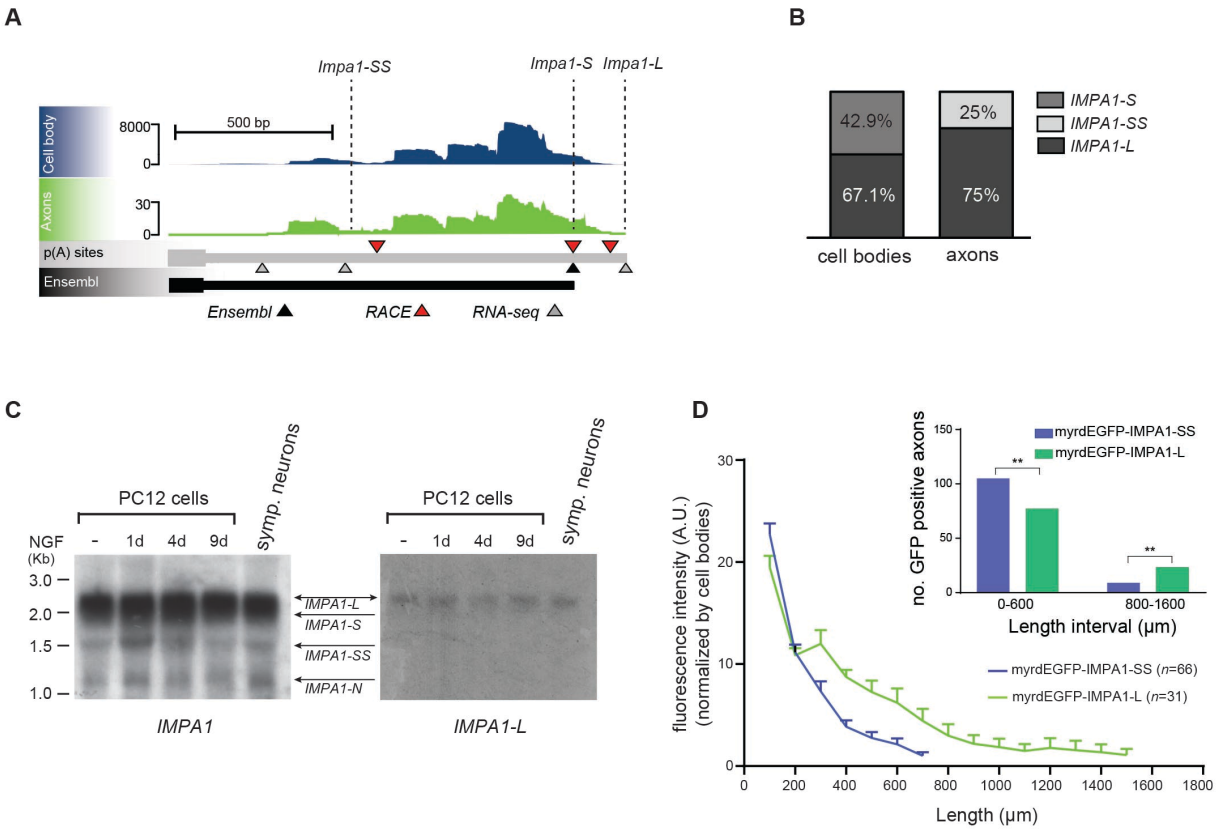

Figure 3: **IMPA1-SS is detected but not transported in axons.** (**A**) Genome browser view of *IMPA1* transcript in NGF and NT-3 treated axons, and cell bodies transcriptomes by 3'end RNA-seq (grey arrowhead) and RACE (red arrowhead). Ensembl annotation (black arrowhead) is also shown. (**B**) RACE of *IMPA1* 3'UTR from transcripts isolated from either cell bodies or axons of sympathetic neurons. Clones from cell bodies 3' RACE carried either *IMPA1-S* (Short) or *IMPA1-L* (Long) 3'UTR. 25% of the clones derived from axon 3' RACE carried *IMPA1-SS* (Super-Short) 3'UTR and the remaining carried *IMPA1-L* 3'UTR. (Cell bodies *n*=15, axons *n*=12). (**C**) Northern blot analysis of RNAs isolated from naïve, NGF-differentiated PC12 cells and sympathetic neurons using ^{32}P-labelled probes annealing with *IMPA1* coding sequence (*Left panel*) or *IMPA-L* 3'UTR (*Right panel)*. (*n*=3). (**D**) Quantitative analysis of GFP protein immunofluorescence in axons of sympathetic neurons expressing either myrdEGFP-IMPA1-L or myrdEGFP-IMPA1-SS. Averages ± s.e.m. of three independent experiments. Inset: Statistical analysis of data in (**D**). Fisher's exact test. **P<0.005. See also **Figure S3**.

Figure 4

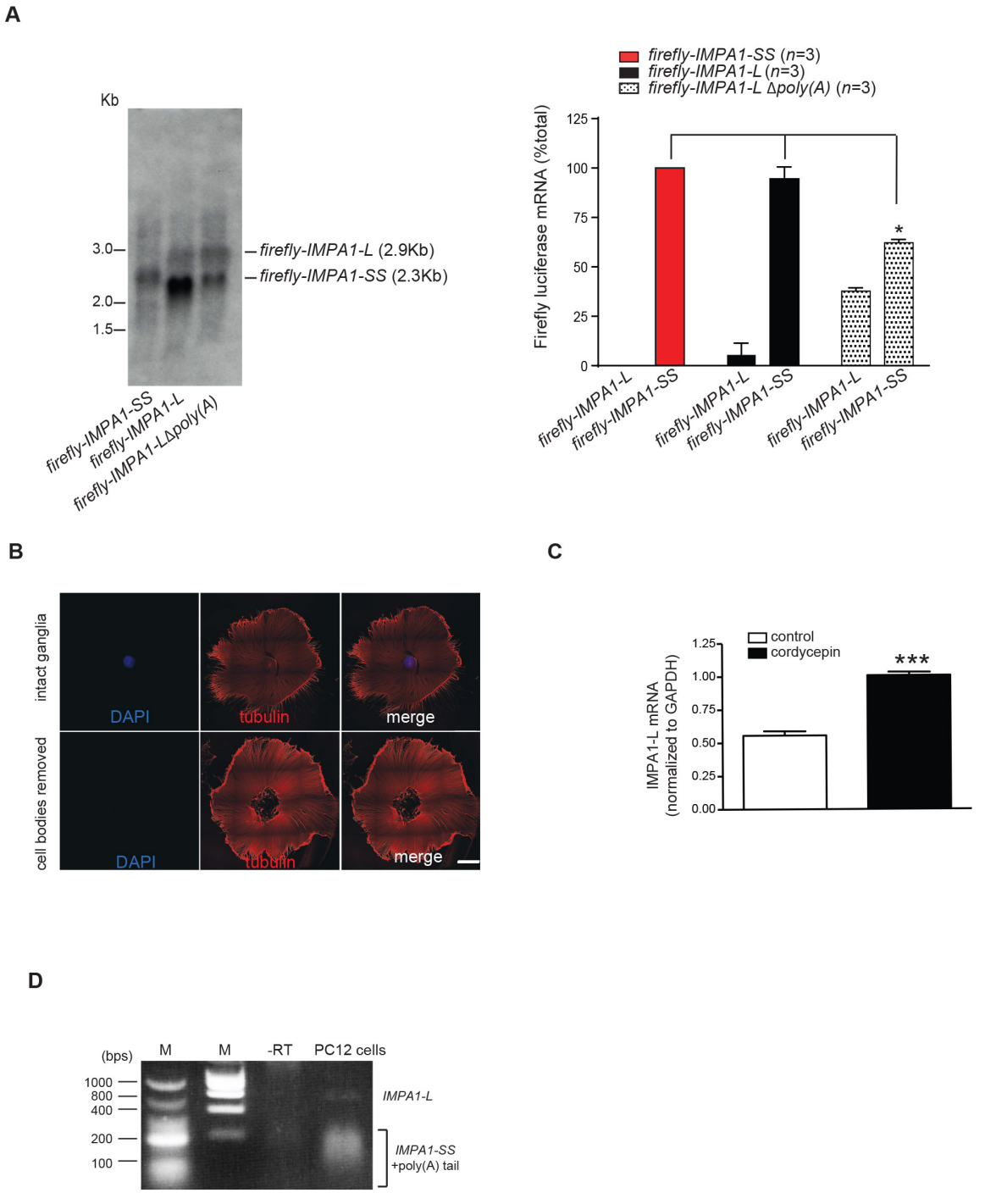

Figure 4: ***IMPA1-SS* is generated by remodelling of *IMPA1-L*.** (**A**) (*Left*) Firefly luciferase northern blotting of PC12 cells transfected with either Firefly-IMPA1-SS, Firefly-IMPA1-L, or Firefly- IMPA1-L ∆p(A) vectors. The lower-than expected molecular weight observed for remodelled *firefly-IMPA1-SS* (compare lanes 2 and 3 to lane 1) may be due to a shorter poly(A) tail of the remodelled *firefly-IMPA1-SS*. (*n*=3). (*Right*) Quantitative analysis of three independent northern blots by phosphorimaging. *P<0.05 multiple t test, statistical significance determined using the Holm-Sidak method, with α=0.05. (**B**) α-Tubulin immunostaining of representative SCG explants before (*Top*) or after (*Bottom*) the removal of cell bodies. Nuclei were stained with DAPI. Scale bar=200μm. (**C**) Cell bodies were removed from SCG explants and axons were exposed to either PBS (control) or cordycepin (2.5μM for 2.5hrs). Expression levels of *IMPA1-L* were tested by qRT-PCR and normalized to *GAPDH*. Values are shown as mean± s.e.m. ***P< 0.001 student t-test (*n*=3). (**D**) mRNA isolated from PC12 cells and subjected to TA-PAT assay to test the length of poly(A) tails on *IMPA1* transcripts. Representative experiment of *n*=3.

Figure 5

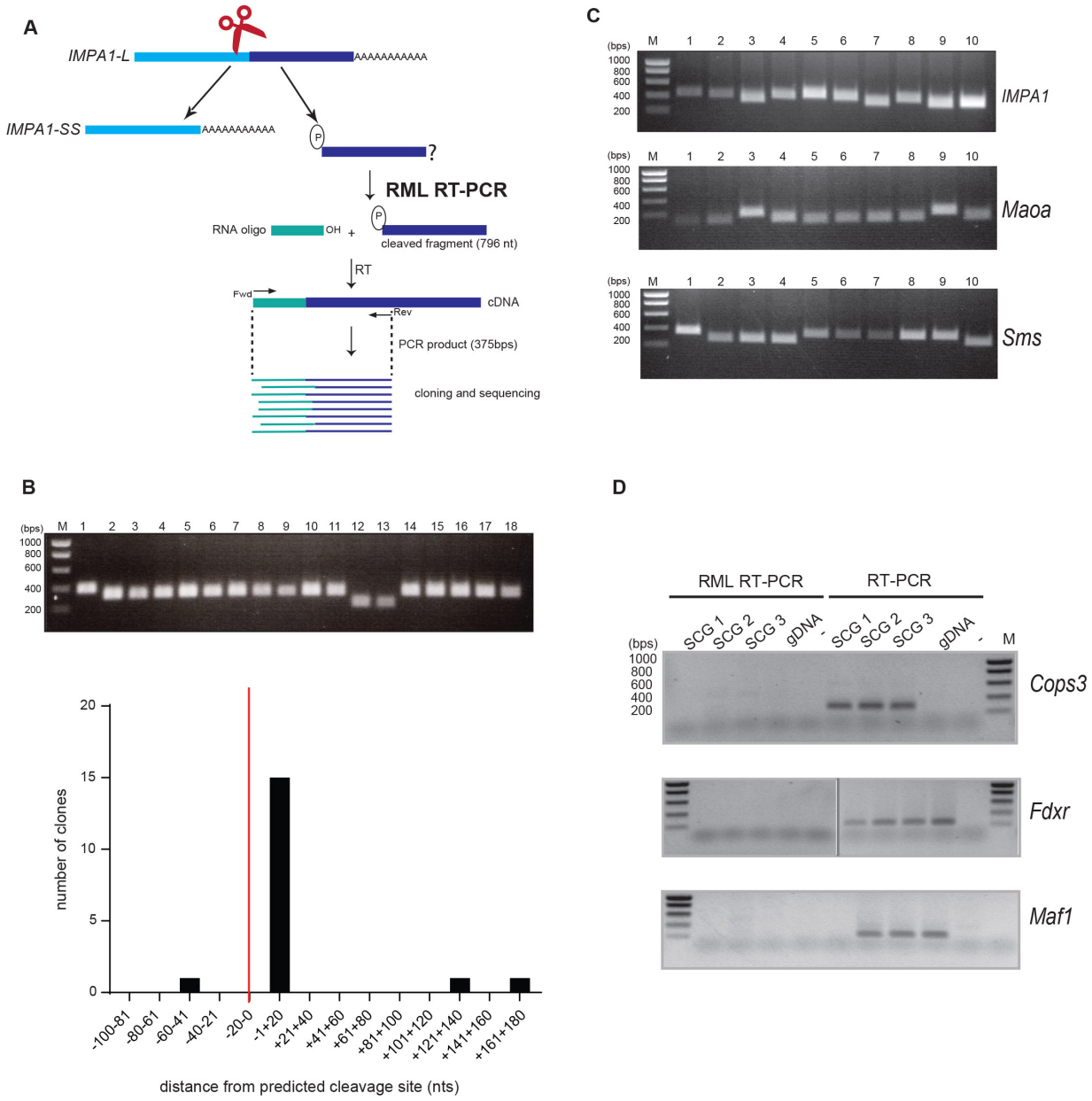

Figure 5: *IMPA1-L* is cleaved in axons to generate *IMPA1-SS*. (A) Schematic representation of 5'P-dependent RNA oligo-Mediated Ligation (RML) experiments. (**B**) (*Top*) Restriction digestions of clones carrying an insert corresponding to *IMPA1-L* cleaved fragment in axons. (*Bottom*) Number of clones of cleaved *IMPA1-L* fragments purified from axonal RNA according to distance from the predicted cleavage site. Each bin=20nts. (**C**) Restriction digestion of representative clones with (*Top*) *IMPA1-L*, (*Middle*) *Maoa* and (*Bottom*) *Sms* cleaved fragments isolated from total cellular RNA by RML RT-PCR. (**D**) (*Left)* Absence of cleaved fragments in *Cops3*, *Fdxr* and *Maf1* transcripts. (*Right*) The presence of corresponding cDNAs was assessed by regular RT-PCR to amplify *Cops3*, *Fdxr* and *Maf1* transcripts. See also **Figure S2**.

Figure 6

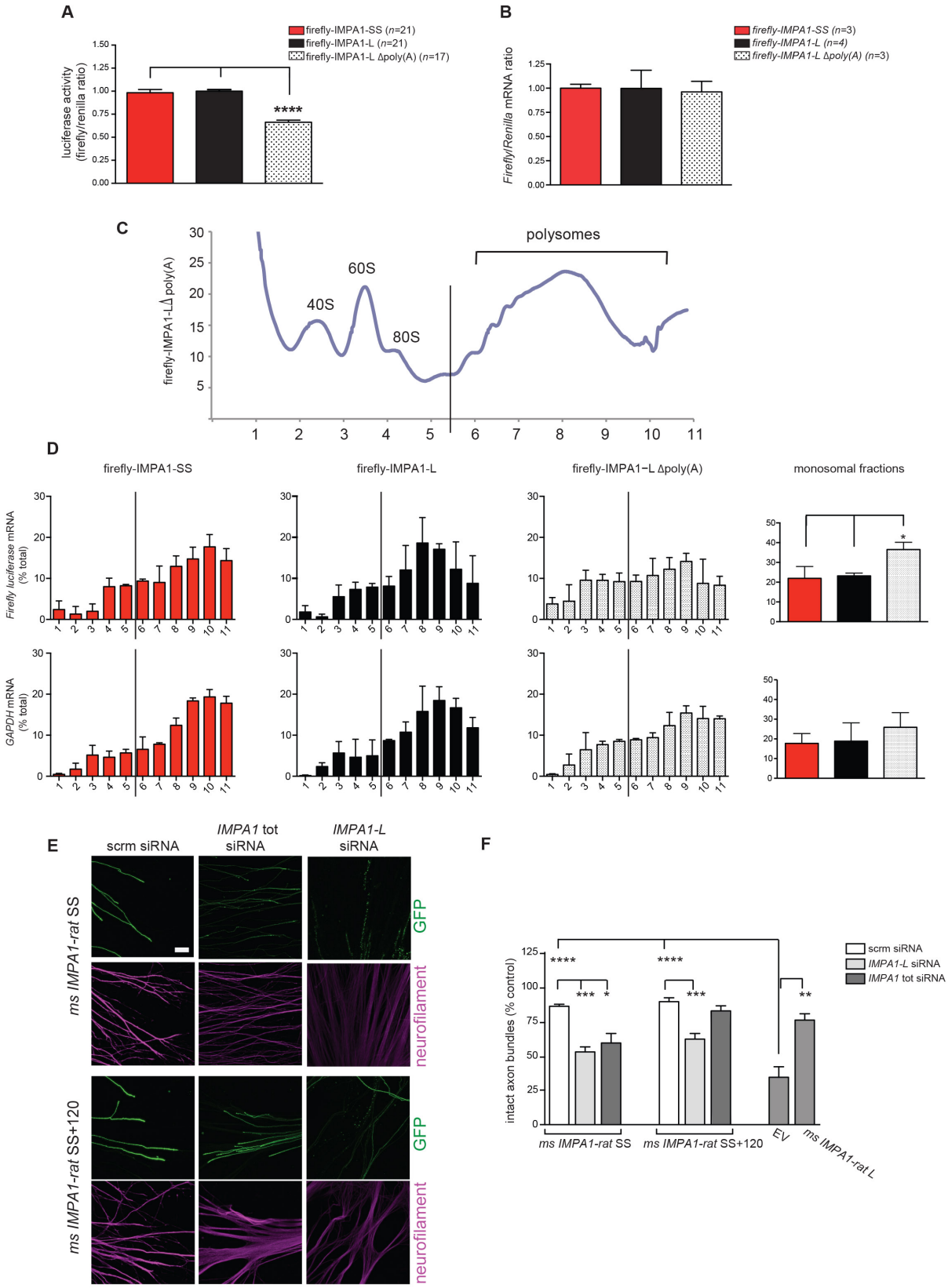

Figure 6: **Mutations *IMPA1* poly(A) sites decrease IMPA1 translation.** (**A**) PC12 cells were transfected with the indicated Firefly Luciferase vectors together with Renilla Luciferase and subjected to luciferase assay. Values are shown as mean ± s.e.m of at least 4 independent experiments. **** P < 0.0001, one-way analysis of variance, Tukey's post hoc test. (**B**) qRT-PCR analysis of *Firefly* and *Renilla luciferase* mRNAs isolated from PC12 cells transfected with the indicated vectors. (**C**) Representative absorbance profile (A254nm) of polysomal fractions isolated from PC12 cells transfected with Firefly-IMPA1L-Δp(A). Peaks representing the 40S, 60S and 80S ribosomal subunits and polysomal fractions are indicated. Line shows separation between free-monosomal and polysomal fractions. (**D**) Lysates of PC12 cells transfected with the indicated Firefly-IMPA1 3'UTR vectors were separated by polysomal fractionation, RNA was isolated from each fraction and subjected to northern analysis using ^{32}P-labeled probes to detect *Firefly* (*Upper graphs*) or *GAPDH* (*Lower graphs*) transcripts. Bands were captured using a phosphorimager and quantified using ImageQuant 5.2 (*right graphs*) (*n*= 3-5). * *p* < 0.01, one-way analysis of variance, Tukey's post hoc test. (**E**) Representative images of SCG explants electroporated with scrambled (scrm) siRNA, total *IMPA1* siRNA, or *IMPA1-L* siRNA, in the presence of ms HA-IMPA1-*rat* IMPA1-SS or *ms* HA-IMPA1-*rat* IMPA1 SS+120, and GFP. Explants were fixed 6 days after electroporation and stained with GFP and neurofilament antibodies. Expression of *ms* HA-IMPA1-*rat* IMPA1SS+120 and of *ms* HA-IMPA1-*rat* IMPA1L, but not of *ms* HA-IMPA1-*rat* IMPA1-SS rescued axonal degeneration induced by total *IMPA1* silencing. Scale bar 75μm.(**F**) Quantitative analysis of the data shown in (**E**). Averages ± s.e.m. of 4 independent experiments. *P < 0.05, **P < 0.005, *** P ≤ 0.001 and ****P < 0.0001 one-way analysis of variance, Tukey's multicomparison test. See also **Figure S3**.

Figure 7

A

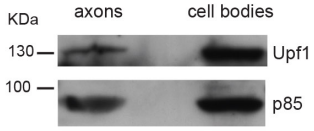

B

Partial list of endogenous Upf1 interactors in PC12 cells identified by mass-spectrometry

UniProt accession number	Description	# Unique Peptides	Median naïve CONT	Median NGF CONT	Enriched in naïve vs.control	Enriched in NGF vs.control	Molecular Function(s)
O09032	ELAV-like protein 4 (HuD)	2	n.d.	100		yes	nucleotide binding; RNA binding: protein binding
G3V6U4	ELAV-like protein 2 (HuB)	1	100	63.4	yes	yes	nucleotide binding; RNA binding
G3V9N0	Polyadenylate-binding protein 4	2	100	100	yes	yes	nucleotide binding; RNA binding
F1LRP7	Protein argonaute-2	2	100	100	yes	yes	RNA binding; catalytic activity; protein binding

C

Upf1:IgG ratio by MS		
protein	näive	+NGF
HuD	n.d.	100
Ago2	100	100
Pabpc4	100	100
Upf1	100	48

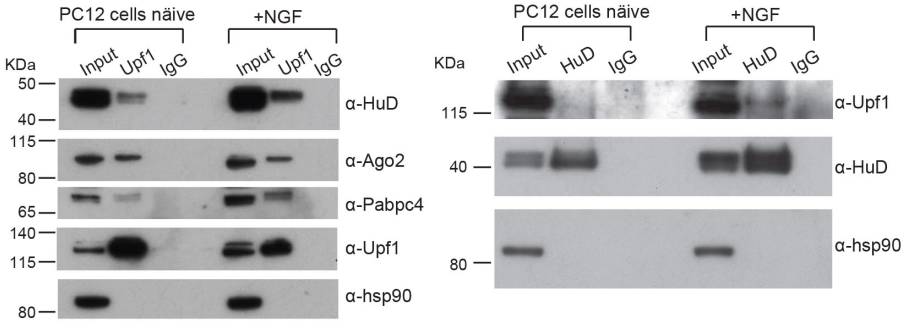

D

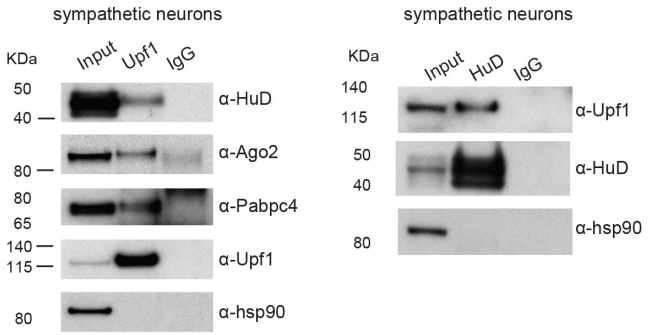

E

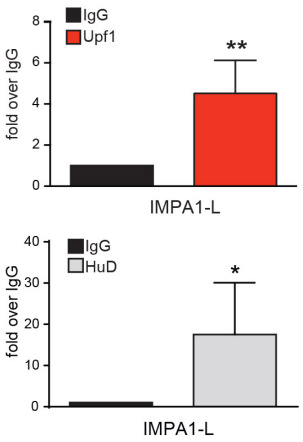

F

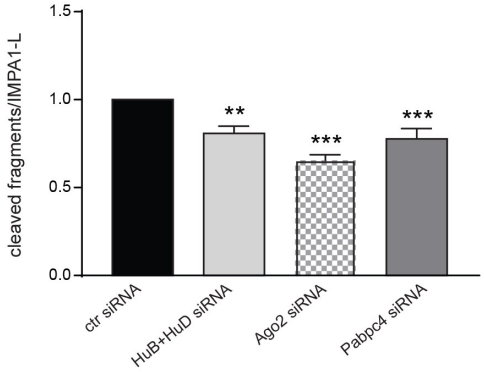

G

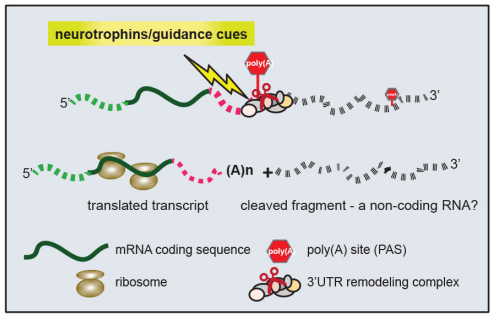

Figure 7: **A Upf1-HuD complex mediates remodelling of *IMPA1* 3'UTR.** (**A**) Western blotting of Upf1 and PI3K subunit p85, as loading control, on axons and cell bodies of sympathetic neurons grown in compartmentalized chambers (*n*=3). (**B**) Partial list of endogenous Upf1 interactors in PC12 cells identified by mass-spectrometry n.d.= not detected. (**C** and **D**) Western blot analysis of Upf1 (*Left*) or HuD (*Right*) immuno-precipitated proteins in extracts of naïve and NGF-differentiated PC12 cells (**C**) or primary sympathetic neurons (**D**). HuD, Ago2 and Pabpc4 co-immuno-precipitate with Upf1. α-tubulin and hsp90 were used as loading controls. (*n*=3). The enrichment of the indicated interactors in the Upf1 immunoprecipitates of naïve or differentiated (+NGF) PC12 cells as measured by mass-spectrometry is shown in the table. (**E**) *IMPA1-L* mRNAs was assayed by qRT-PCR on sympathetic neuron lysates immunoprecipitated with normal IgG or Upf1 antibody (*Top*), or normal IgG and HuD antibody (*Bottom*). (*n*=3) *P< 0.05, **P<0.005 unpaired one-tailed t test. (**F**) Silencing of Upf1 interacting proteins decreases the remodelling of IMPA1-L 3'UTR. *IMPA1-L* cleavage was assayed by RML qRT-PCR on RNA purified from PC12 cells transfected with the indicated siRNAs. Averages ± s.e.m. of at least 3 independent experiments *** P < 0.0005 and **P < 0.005, one-way analysis of variance, Dunnett's multiple comparison test. See also **Figure S5**.

Figure S1

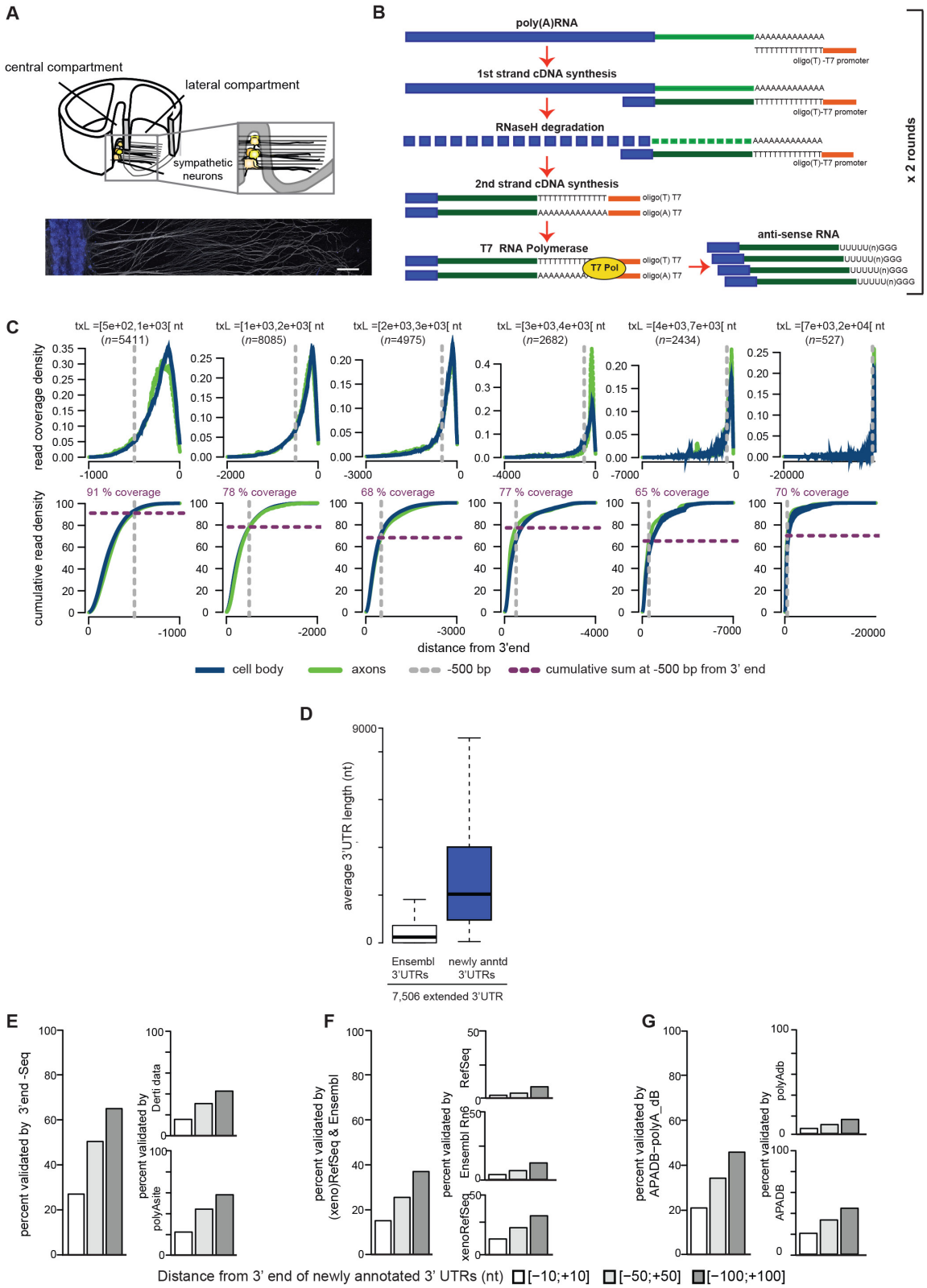

Figure S1: **3' end-RNA-seq of linearly amplified RNA from axons and cell bodies of sympathetic neurons.** Related to **Figure 1**. (**A**) (*Upper panel*) Schematic representation of a compartmentalized chamber. Neurons are plated in the central compartment and axons grow into the lateral compartments. (*Lower panel*) Immunofluorescence of sympathetic neurons grown in compartmentalized chambers for 10 days and stained with DAPI (blue) and β-tubulin (white) antibody. Scale bar 500μm. (**B**) Schematic representation of linear amplification of mRNA. (**C**) Reads accumulation at 3' end of the Ensembl transcripts in function of transcript length. (*Upper*) Read density coverage and (*Lower*) cumulative read density along transcript are shown. (**D**) Average length of the 3'UTRs of 7,506 Ensembl transcript ID extended by intersecting expressed genomic fragments with Ensembl Rn5 annotation. (**E-G**) Percentage of 3'UTR isoforms for which the indicated region surrounding the 3' end intersects with a PAS obtained from 3'-Seq data (**E**), a 3' termini annotated in RefSeq (Rn5, Rn6 and XenoRefSeq) or Ensembl (Rn6) (**F**), or a PAS annotated in APADB or PolyA-DB2 (**G**). Comparison between combined (*Left*) and individual (*Right*) datasets is shown in each panel.

Figure S2

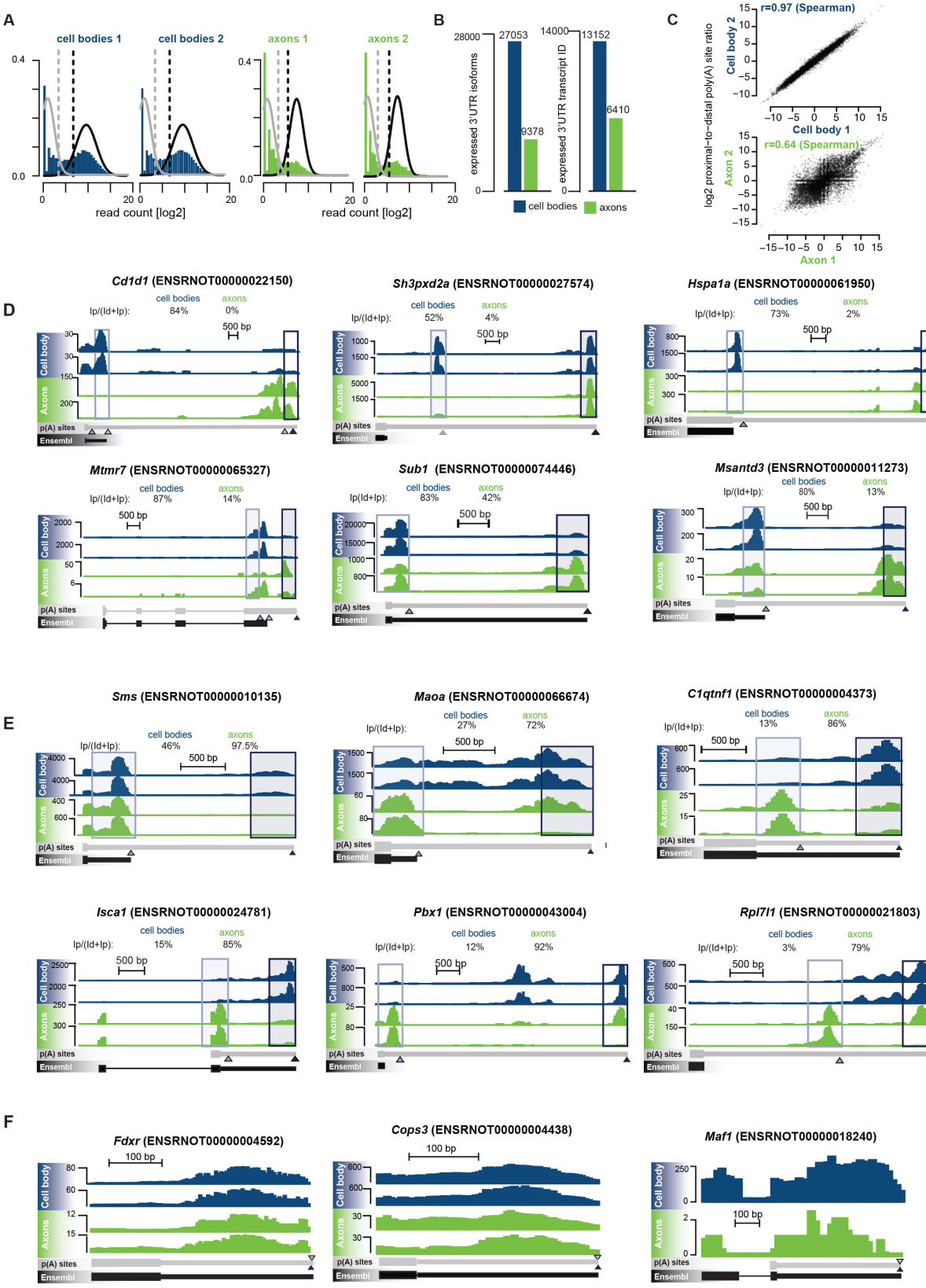

Figure S2: **Analysis of 3'UTR length and PAS choice in axonal and cell bodies transcriptomes.** Related to **Figure 2**. (**A**) Identification of 3'UTR isoforms expressed in cell bodies (blue) and axons (green) performed by fitting bimodal distribution on log2-raw count mapping the 500 nts distal region of 3' end. (**B**) Number of 3'UTR isoforms (*left*) and Ensembl transcript ID (*right*) expressed in cell bodies and axons. (**C**) Scatter plots of the relative use of promoter-proximal and promoter-distal poly(A) sites in two biological replicates each of cell bodies (upper panel) and axons (lower panel) samples. (**D** and **E**) Examples of transcripts with a marked shift towards increased promoter-distal poly(A) site usage in axons compared to cell bodies (**D**) or with a marked shift towards increased promoter-proximal poly(A) site usage in axons compared to cell bodies (**E**). (**F**) Examples of 3 transcripts with single 3'UTR isoforms.

Figure S3

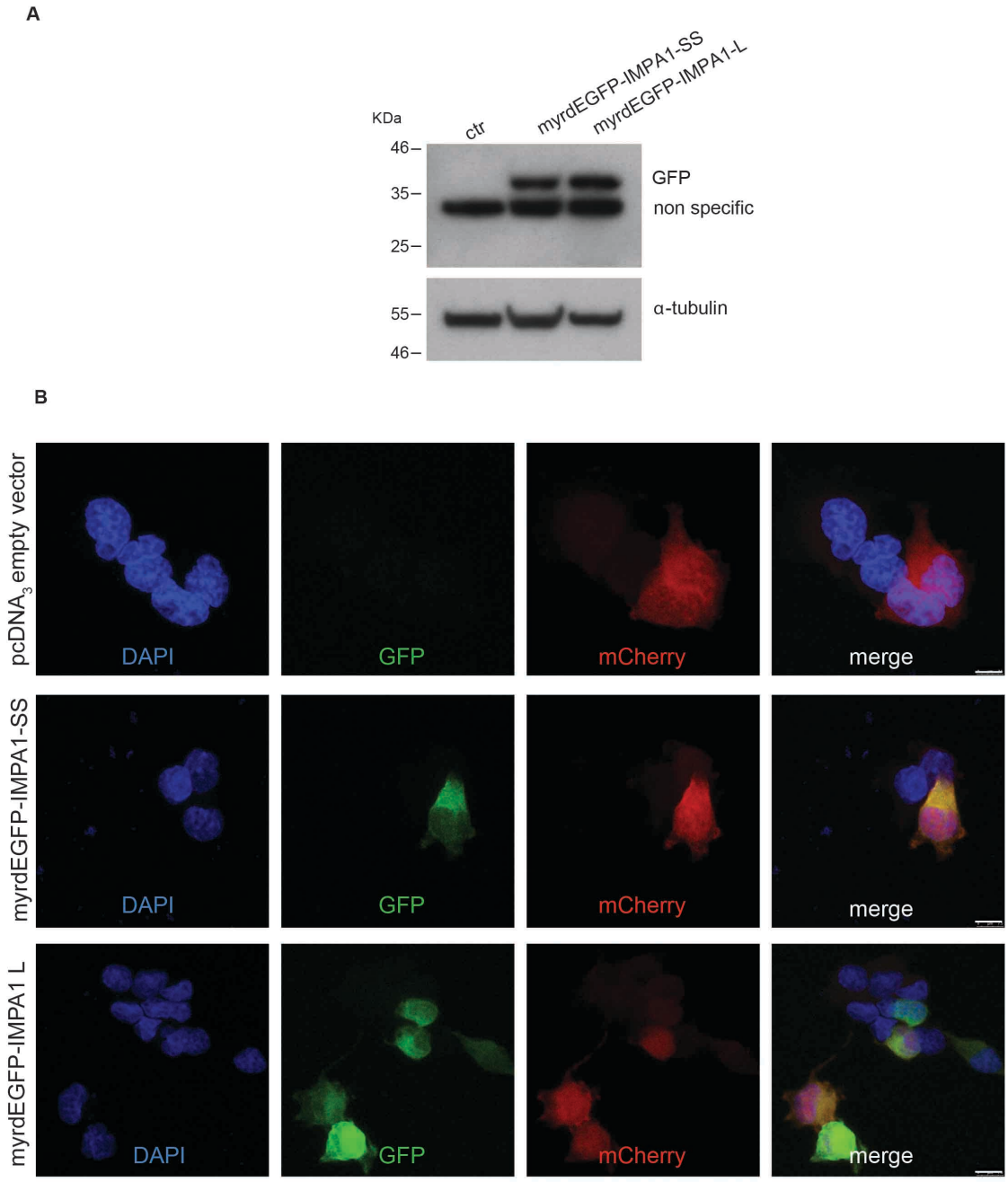

Figure S3. Controls for construct expression and antibody specificity. Related to **Figure 3.** (**A**) Western blotting analysis of GFP and α–tubulin on protein extracts of PC12 cells transfected with either MyrdEGFP-Impa1-L or MyrdEGFP-Impa1-SS. Ctr: non transfected cells. (**B**) Representative images of naïve PC12 cells transfected with empty vector pcDNA3 or myrdEGFP-IMPA1SS or myrdEGFP-IMPA1L, and mCherry plasmids. Cells were fixed 3 days after transfection and stained with GFP and DsRed antibodies. Nuclei are counterstained with DAPI. The non specific band present in western blot (**A**) does not affect immunofluorescence staining. Scale bar 75μm. (*n*=3).

Figure S4

A

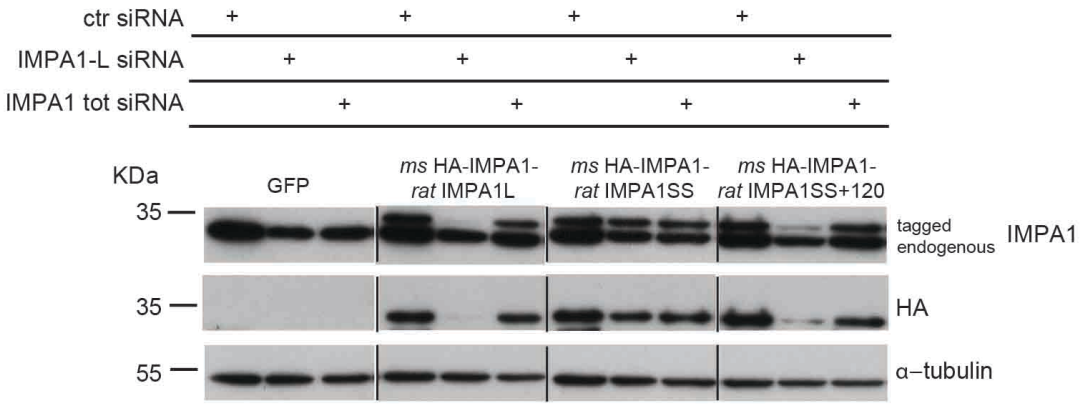

B

DNA vectors	Transported to axons	Targeted by ctr siRNA	Targeted by IMPA1 total siRNA	Targeted by IMPA1-L siRNA
Empty Vector EV	n.a.	✗	✗	✗
ms HA-IMPA1-rat L	✓	✗	✗	✓
ms HA-IMPA1-rat SS	✗	✗	✗	✗
ms HA-IMPA1-rat SS+120	✓	✗	✗	✓

n.a.=not applicable ✗=no ✓=yes

Figure S4: **Specificity of silencing and rescue constructs.** Related to **Figure 6**. (**A**) IMPA1, hemagglutinin (HA) and α-tubulin western blotting of PC12 cells transfected with the indicated siRNAs and vectors encoding HA-tagged mouse IMPA1 with either the long, the super-short or the super-short+ IMPA1L localization signal (SS+120) rat Impa1 3′ UTR (*ms* HA-IMPA1-*rat* IMPA1L, *ms*-HA IMPA1-*rat* IMPA1-SS and *ms* HA-Impa1-*rat* IMPA1 SS+120, respectively). Higher band in top panels is HA-tagged mouse IMPA1 and lower band is endogenous rat IMPA1 (*n*= 3). (**B**) Summary table of the localization ability and silencing susceptibility of the constructs used in **A** and in **Figure 6**.

Figure S5

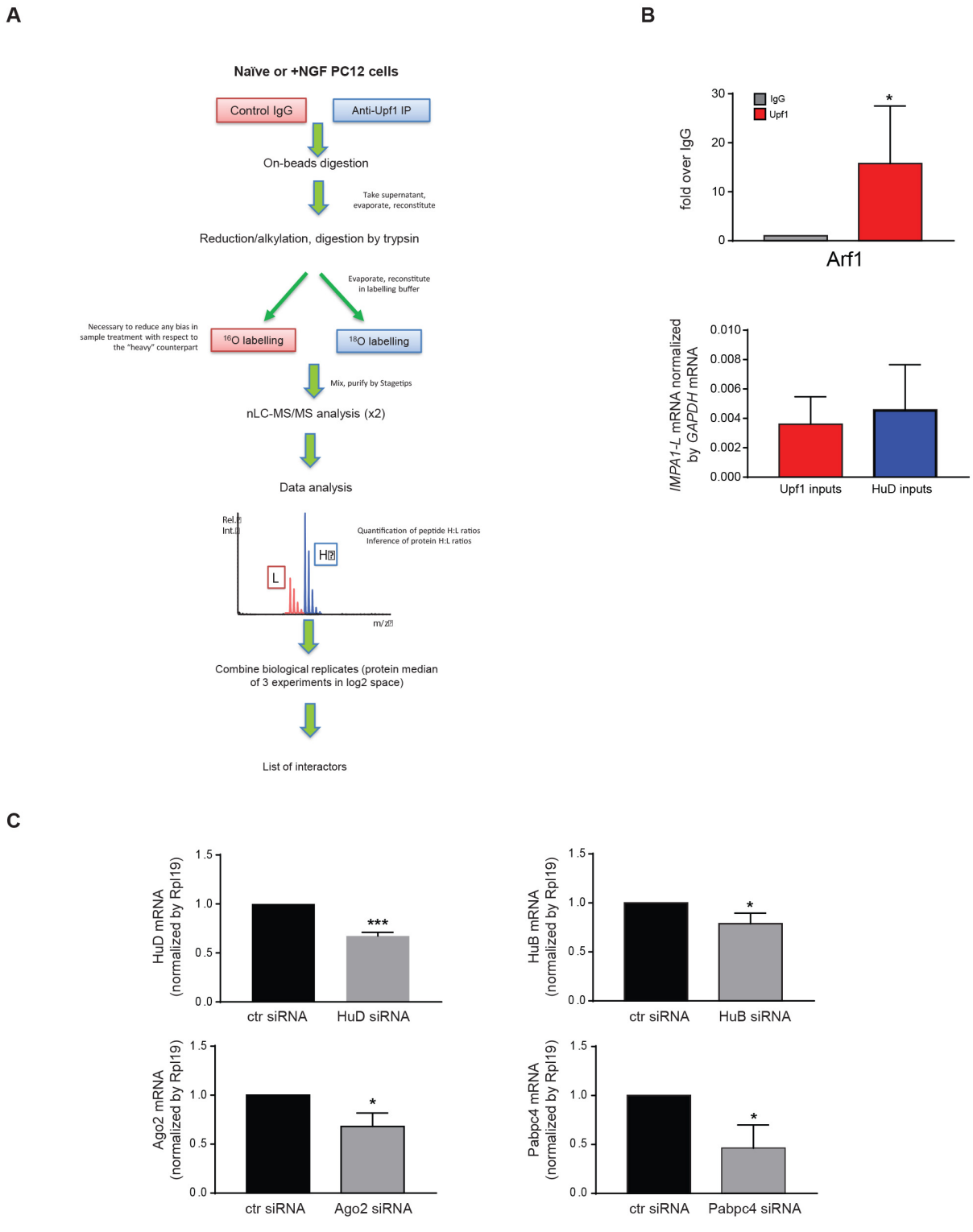

Figure S5. **Remodelling of IMPA1 3'UTR depends on Upf1 and HuD complexes.** Related to **Figure 7**. (**A**) Workflow employed for the discovery of UPF1 interactors in naïve and NGF-stimulated cells. (**B**) *Arf1* mRNA was quantified by qRT-PCR in sympathetic neurons lysates immunoprecipitated with normal IgG or Upf1 antibody (*top*). Normalized expression of *IMPA1-L* in sympathetic neurons lysates used in RIP experiments (*bottom*). (n=4). *P < 0.05 unpaired one-tail t-test. (**C**) RT-qPCR to evaluate efficiency of *HuB*, *HuD*, *Ago2* and *Pabpc4* silencing. n=4-6. * P < 0.05, ** P < 0.005, *** P < 0.0005 Paired t-test.